

Study of new physics effects in $\bar{B}_s \rightarrow D_s^{(*)} \tau^- \bar{\nu}_\tau$ semileptonic decays using Standard Model lattice QCD form factors and heavy quark effective theory

Neus Penalva,¹ Jonathan M. Flynn,² Eliecer Hernández,³ and Juan Nieves¹

¹*Instituto de Física Corpuscular (centro mixto CSIC-UV), Institutos de Investigación de Paterna, C/Catedrático José Beltrán 2, E-46980 Paterna, Valencia, Spain*

²*Physics & Astronomy, University of Southampton, Southampton SO17 1BJ, UK*

³*Departamento de Física Fundamental e IUFFyM, Universidad de Salamanca, Plaza de la Merced s/n, E-37008 Salamanca, Spain*

(Dated: April 4, 2023)

We benefit from the lattice QCD determination of the Standard Model (SM) form factors for the $\bar{B}_s \rightarrow D_s^*$ and $\bar{B}_s \rightarrow D_s$ semileptonic decays carried out by the HPQCD collaboration in Refs. Phys. Rev. D 105, 094506 (2022) and Phys. Rev. D 101, 074513 (2020), and the heavy quark effective theory (HQET) relations for the analogous $B \rightarrow D^{(*)}$ decays obtained by F.U. Bernlochner et al. in Phys. Rev. D 95, 115008 (2017), to extract the leading and sub-leading Isgur-Wise functions for the $\bar{B}_s \rightarrow D_s^{(*)}$ decays. Further use of the HQET relations allows us to evaluate the corresponding scalar, pseudoscalar and tensor form factors needed for a phenomenological study of new physics (NP) effects on the $\bar{B}_s \rightarrow D_s^{(*)}$ semileptonic decay. At present, the experimental values for the ratios $\mathcal{R}_{D^{(*)}} = \Gamma[\bar{B} \rightarrow D^{(*)} \tau^- \bar{\nu}_\tau] / \Gamma[\bar{B} \rightarrow D^{(*)} e^- (\mu^-) \bar{\nu}_{e(\mu)}]$ are the best signal in favor of lepton flavor universality violation (LFUV) seen in charged current (CC) $b \rightarrow c$ decays. In this work we conduct a study of NP effects on the $\bar{B}_s \rightarrow D_s^{(*)} \tau^- \bar{\nu}_\tau$ semileptonic decays by comparing tau spin, angular and spin-angular asymmetry distributions obtained within the SM and three different NP scenarios. As expected from SU(3) light-flavor symmetry, we get results close to the ones found in a similar analysis of the $\bar{B} \rightarrow D^{(*)}$ case. The measurement of the $\bar{B}_s \rightarrow D_s^{(*)} \ell \bar{\nu}_\ell$ semileptonic decays, which is within reach of present experiments, could then be of relevance in helping to establish or rule out LFUV in CC $b \rightarrow c$ transitions.

I. INTRODUCTION

Present experimental data on $\bar{B} \rightarrow D^{(*)}$ semileptonic decays points to the possibility of lepton flavor universality violation (LFUV) that will affect charged-current (CC) $b \rightarrow c\tau^-\bar{\nu}_\tau$ semileptonic transitions. The ratios $\mathcal{R}_D = \Gamma(\bar{B} \rightarrow D\tau^-\bar{\nu}_\tau)/\Gamma(\bar{B} \rightarrow D\mu^-\bar{\nu}_\mu)$ and $\mathcal{R}_{D^*} = \Gamma(\bar{B} \rightarrow D^*\tau^-\bar{\nu}_\tau)/\Gamma(\bar{B} \rightarrow D^*\mu^-\bar{\nu}_\mu)$ have been measured by the BaBar [1, 2], Belle [3–6] and LHCb [7–10] experiments and their combined analysis by the HFLAV collaboration indicates a 3σ tension with SM predictions [11, 12].

LFUV requires the existence of new physics (NP) beyond the Standard Model (SM) and, if confirmed, would have a tremendous impact in particle physics. This makes the study of as many analogous CC decays as possible timely and necessary in order to confirm or rule out LFUV. The $\mathcal{R}_{J/\psi} = \Gamma(\bar{B}_c \rightarrow J/\psi\tau^-\bar{\nu}_\tau)/\Gamma(\bar{B}_c \rightarrow J/\psi\mu^-\bar{\nu}_\mu)$ ratio has been measured by the LHCb collaboration [13] finding a 1.8σ discrepancy with SM results [14–26]. Another reaction where a similar behavior was to be expected is the baryon $\Lambda_b \rightarrow \Lambda_c\ell\bar{\nu}_\ell$ decay. However, in this case, the recent measurement of the $\mathcal{R}_{\Lambda_c} = \Gamma(\Lambda_b \rightarrow \Lambda_c\tau^-\bar{\nu}_\tau)/\Gamma(\Lambda_b \rightarrow \Lambda_c\mu^-\bar{\nu}_\mu)$ ratio by the LHCb collaboration [27] is in agreement, within errors, with the SM prediction [28]. In this experiment, the τ^- lepton was reconstructed using the $\tau^- \rightarrow \pi^-\pi^+\pi^-(\pi^0)\nu_\tau$ hadronic decay. It is then of great interest to see whether the current \mathcal{R}_{Λ_c} experimental value is confirmed or not using the muonic reconstruction channel. Such an analysis is under way [29].

LHCb has very recently [10] presented the first simultaneous measurement in hadron collisions of \mathcal{R}_{D^*} and \mathcal{R}_{D^0} , identifying the tau lepton from its the decay mode $\tau^- \rightarrow \mu^-\nu_\tau\bar{\nu}_\mu$. The measured values are $\mathcal{R}_{D^*} = 0.281 \pm 0.018 \pm 0.024$ and $\mathcal{R}_{D^0} = 0.441 \pm 0.060 \pm 0.066$, where the correlation between these measurements is -0.43 . The result for the former ratio supersedes the higher value previously reported in [7] and it is now in better agreement with the SM. LHCb earlier measured $\mathcal{R}_{D^*} = 0.291 \pm 0.019 \pm 0.026 \pm 0.013$ [8, 9] using hadronic tau decays, but a new result in preparation and reported in [12], $\mathcal{R}_{D^*} = 0.257 \pm 0.012 \pm 0.014 \pm 0.012$, is in closer agreement with the SM expectation. Nevertheless combined global results for \mathcal{R}_{D^*} and \mathcal{R}_D from different experiments and detection techniques remain around 3σ away from the SM expectation (HFLAV Winter 2023 update [30] presented in [12]).

One would also expect to see LFUV effects in $\bar{B}_s \rightarrow D_s^{(*)}$ semileptonic decays which are SU(3) analogues of the $\bar{B} \rightarrow D^{(*)}$ ones. A measurement of \mathcal{R}_{D_s} by LHCb [12] is also underway, making the study of these reactions timely. The theoretical analysis of NP effects in those decays requires however knowledge of beyond-the-SM (BSM) form factors that have not yet been determined. SM form factors for the $\bar{B}_s \rightarrow D_s^{(*)}$ semileptonic transitions have been evaluated on the lattice in Refs. [31, 32]. In addition, the approximate heavy quark spin symmetry (HQSS) of QCD allows one to construct an effective field theory (HQET) to compute these form-factors. Indeed, the HQSS expressions for them can be obtained from Ref. [33], where they were derived for the $\bar{B} \rightarrow D^{(*)}$ decays. One can use this information to fit the leading and sub-leading HQSS Isgur-Wise (IW) functions, which describe the $\bar{B}_s \rightarrow D_s^{(*)}$ form factors, to the SM lattice data and quantify the size of the SU(3) light-flavor breaking corrections.

Once the IW functions are known, one can use the HQSS relations to obtain the scalar, pseudoscalar and tensor form factors that are needed in addition to the SM ones for an analysis of possible NP effects on the $\bar{B}_s \rightarrow D_s^{(*)}$ decays. This is what we have done in this work which is organized as follows. In Sec. II we describe the fitting procedure to obtain the IW functions, with some auxiliary details collected in the Appendix. A thorough analysis of NP effects, based on observables that can be measured by the analysis of the visible kinematics of the subsequent hadronic $\tau^- \rightarrow \pi^-\nu_\tau, \tau^- \rightarrow \rho^-\nu_\tau$ and leptonic $\tau^- \rightarrow \ell^-\bar{\nu}_\ell\nu_\tau$ decays, is conducted in Sec. III. Finally in Sec. IV we summarize the main findings.

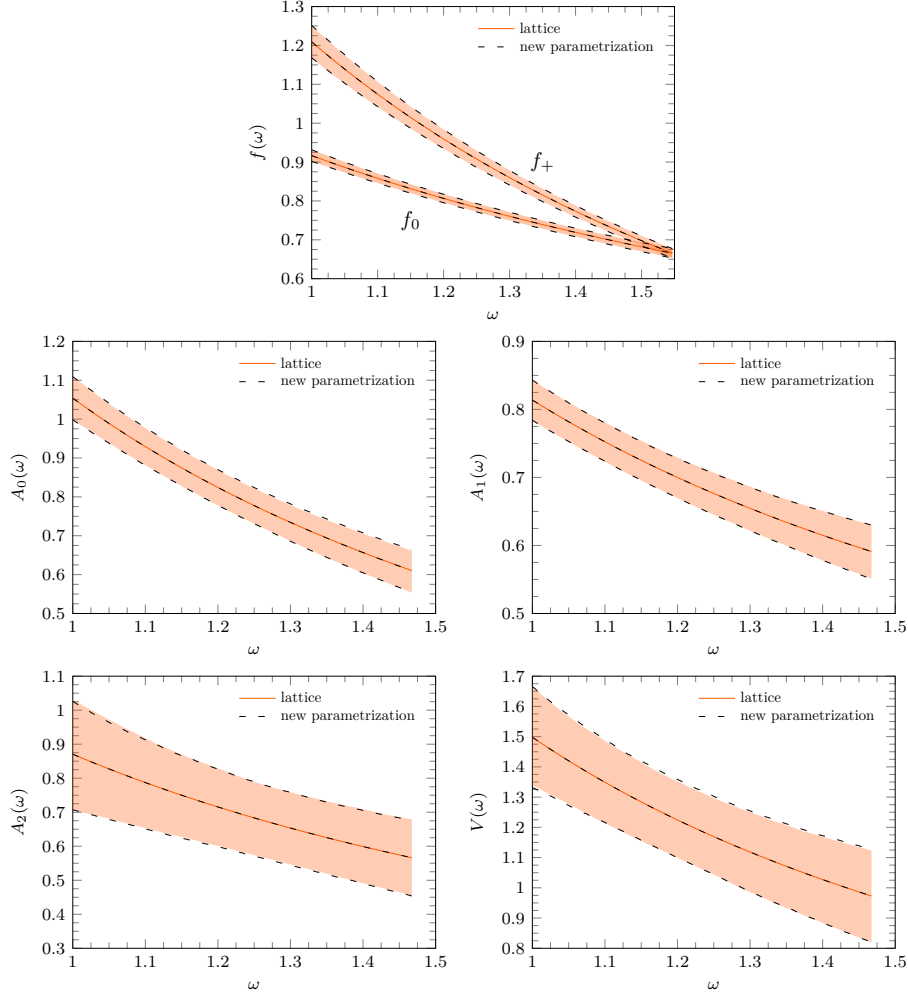


FIG. 1. Comparison of the original SM-LQCD form factors for $\bar{B}_s \rightarrow D_s$ [31] and $\bar{B}_s \rightarrow D_s^*$ [32] and their description in this work using the parametrizations of Eqs. (12) and (10), respectively. Both central values and 68% confidence level (CL) bands show excellent agreement.

II. HQET FIT OF THE $\bar{B}_s \rightarrow D_s^{(*)}$ SEMILEPTONIC-DECAY SM-LQCD FORM FACTORS AND SM DISTRIBUTIONS

In this section we will describe how we fit the SM-LQCD form-factor data from Refs. [31, 32] to their expressions expected from HQET and derived in Ref. [33]. A comparison of both sets of form factors is done by showing their predictions for differential decay widths and tau spin, angular and spin-angular asymmetry distributions. Further use of HQSS will allow us to predict BSM form factors which we will use in the next section to test for possible NP effects in $\bar{B}_s \rightarrow D_s^{(*)} \tau^- \bar{\nu}_\tau$ semileptonic decays.

A. LQCD form factors

We will use LQCD results from HPQCD for the SM form factors for $\bar{B}_s \rightarrow D_s^*$ [32] and $\bar{B}_s \rightarrow D_s$ [31] semileptonic decays. The results are presented as coefficients in power series of a conformal

variable

$$z(q^2; t_{\text{th}}, t_0) = \frac{\sqrt{t_{\text{th}} - q^2} - \sqrt{t_{\text{th}} - t_0}}{\sqrt{t_{\text{th}} - q^2} + \sqrt{t_{\text{th}} - t_0}}, \quad (1)$$

where q^μ is the four-momentum transfer to the leptons and the choices made for t_{th} and t_0 are given below. For the $\bar{B}_s \rightarrow D_s^*$ decay, the authors of Ref. [32] use the following decomposition of the current matrix elements

$$\begin{aligned} \langle D_s^*; \vec{p}', r | \bar{c}(0) \gamma^\mu b(0) | \bar{B}_s; \vec{p} \rangle &= \frac{2iV(q^2)}{M_{B_s} + M_{D_s^*}} \epsilon^{\mu\nu\rho\sigma} \epsilon_\nu^*(\vec{p}', r) p'_\rho p_\sigma, \\ \langle D_s^*; \vec{p}' | \bar{c}(0) \gamma^\mu \gamma_5 b(0) | \bar{B}_s; \vec{p} \rangle &= 2M_{D_s^*} A_0(q^2) \frac{\epsilon^*(\vec{p}', r) \cdot q}{q^2} q^\mu \\ &\quad + (M_{B_s} + M_{D_s^*}) A_1(q^2) \left[\epsilon^{*\mu}(\vec{p}', r) - \frac{\epsilon^*(\vec{p}', r) \cdot q}{q^2} q^\mu \right] \\ &\quad - A_2(q^2) \frac{\epsilon^*(\vec{p}', r) \cdot q}{M_{B_s} + M_{D_s^*}} \left[p^\mu + p'^\mu - \frac{M_{B_s}^2 - M_{D_s^*}^2}{q^2} q^\mu \right], \end{aligned} \quad (2)$$

with $\epsilon_{0123} = +1$. The different form factors have been parametrized by¹

$$F(q^2) = \frac{1}{P_F(q^2)} \sum_{n=0}^3 \tilde{a}_n^F(z^*)^n \quad (3)$$

with

$$\tilde{z}^*(q^2) = z(q^2; t_{\text{th}}, t_0), \quad t_{\text{th}} = (M_B + M_{D_s^*})^2, \quad t_0 = (M_{B_s} - M_{D_s^*})^2. \quad (4)$$

The $P_F(q^2)$ factors account for poles corresponding to $b\bar{c}$ states with masses below the pair production threshold t_{th} . Their expressions can be found in Ref. [32]. The absence of a singularity at $q^2 = 0$ leads to the constraint

$$2M_{D_s^*} A_0(0) = (M_{B_s} + M_{D_s^*}) A_1(0) + (M_{D_s^*} - M_{B_s}) A_2(0). \quad (5)$$

The central values and errors for the \tilde{a}_i^F expansion coefficients in Eq. (3), as well as the corresponding correlation matrix are given, respectively, in Table XIII and Tables XXII-XXXI of Ref. [32].

For the $\bar{B}_s \rightarrow D_s$ semileptonic decay, the form-factor decomposition is [31]

$$\langle D_s; \vec{p}' | \bar{c}(0) \gamma^\mu b(0) | \bar{B}_s; \vec{p} \rangle = f_+(q^2) \left[p^\mu + p'^\mu - \frac{M_{B_s}^2 - M_{D_s}^2}{q^2} q^\mu \right] + f_0(q^2) \frac{M_{B_s}^2 - M_{D_s}^2}{q^2} q^\mu, \quad (6)$$

with the constraint

$$f_0(0) = f_+(0). \quad (7)$$

The form factors are parametrized in [31] by

$$\begin{aligned} f_0(q^2) &= \frac{1}{1 - q^2/M_{B_{c0}}^2} \sum_{n=0}^2 \tilde{a}_n^0 \tilde{z}^n, \\ f_+(q^2) &= \frac{1}{1 - q^2/M_{B_c^*}^2} \sum_{n=0}^2 \tilde{a}_n^+ \left[\tilde{z}^n - \frac{(-1)^{n-3} n}{3} \tilde{z}^3 \right], \end{aligned} \quad (8)$$

¹ In contrast to the original works in Refs. [31, 32], we use tilde's to denote z -variables and a coefficients of the HPQCD form-factor parametrizations.

with

$$\tilde{z}(q^2) = z(q^2; t_{\text{th}}, 0), \quad t_{\text{th}} = (M_{B_s} + M_{D_s})^2. \quad (9)$$

The constraint in Eq. (7) imposes $\tilde{a}_0^0 = \tilde{a}_0^+$.

For our HQSS fit of the form factors we change the parametrizations above to symmetrize the range of z corresponding to $0 \leq q^2 \leq t_-^{(*)}$ where $t_-^{(*)} = (M_{B_s} - M_{D_s}^{(*)})^2$ for the two decays. For $\bar{B}_s \rightarrow D_s^*$ we use

$$F(q^2) = \frac{1}{P_F(q^2)} \sum_{n=0}^3 a_n^F (z^*)^n \quad (10)$$

with

$$z^*(q^2) = z(q^2; t_{\text{th}}, t_0), \quad t_{\text{th}} = (M_B + M_{D^*})^2, \quad t_0 = t_{\text{th}} - \sqrt{t_{\text{th}}(t_{\text{th}} - t_-^*)}. \quad (11)$$

For $\bar{B}_s \rightarrow D_s$ we use

$$f_0(q^2) = \frac{1}{1 - q^2/M_{B_c^0}^2} \sum_{n=0}^2 a_n^0 z^n, \quad f_+(q^2) = \frac{1}{1 - q^2/M_{B_c^*}^2} \sum_{n=0}^2 a_n^+ z^n, \quad (12)$$

with

$$z(q^2) = z(q^2; t_{\text{th}}, t_0), \quad t_{\text{th}} = (M_B + M_D)^2, \quad t_0 = t_{\text{th}} - \sqrt{t_{\text{th}}(t_{\text{th}} - t_-)}. \quad (13)$$

The central values and errors of the new expansion coefficients, together with the corresponding correlation matrices, are collected in Tables VI–XVII of the Appendix. We use Eq. (5) to fix the $a_3^{A_2}$ coefficient for $\bar{B}_s \rightarrow D_s^*$ and Eq. (7) to fix a_2^+ for $\bar{B}_s \rightarrow D_s$. The quality of these new expansions can be seen in Fig. 1 where we compare them to the lattice form factors obtained in Refs. [31, 32]. The agreement is excellent.

B. HQSS form factors

In HQET, one normally uses the following form-factor decomposition of the transition-current matrix elements [33]

$$\begin{aligned} \langle D_s^*; \vec{p}', r | \bar{c}(0) \gamma^\mu b(0) | \bar{B}_s; \vec{p} \rangle &= i \sqrt{M_{B_s} M_{D_s^*}} h_V(q^2) \epsilon^{\mu\nu\rho\sigma} \epsilon_\nu^*(\vec{p}', r) v'_\rho v_\sigma, \\ \langle D_s^*; \vec{p}' | \bar{c}(0) \gamma^\mu \gamma_5 b(0) | \bar{B}_s; \vec{p} \rangle &= \sqrt{M_{B_s} M_{D_s^*}} \{ h_{A_1}(q^2) (\omega + 1) \epsilon^{*\mu}(\vec{p}', r) - h_{A_2}(q^2) [\epsilon^{*\mu}(\vec{p}', r) \cdot v] v^\mu \\ &\quad - h_{A_3}(q^2) [\epsilon^{*\mu}(\vec{p}', r) \cdot v] v'^\mu \} \\ \langle D_s; \vec{p}' | \bar{c}(0) \gamma^\mu b(0) | \bar{B}_s; \vec{p} \rangle &= \sqrt{M_{B_s} M_{D_s}} [h_+(q^2) (v^\mu + v'^\mu) + h_-(q^2) (v^\mu - v'^\mu)], \end{aligned} \quad (14)$$

with v, v' the four-velocities of the initial and final hadron respectively. The h_i form-factors depend on q^2 , or equivalently on $\omega = v \cdot v'$.

In Ref. [33] the above form factors have been computed in the effective field theory, up to $\mathcal{O}(\alpha_s, \Lambda_{\text{QCD}}/m_{c,b})$ corrections, for the analogous $\bar{B} \rightarrow D^{(*)}$ semileptonic decays. We take advantage of this study and use the findings of Ref. [33] to describe the $\bar{B}_s \rightarrow D_s^{(*)}$ form-factors. In the infinite heavy quark mass limit the form factors are given by the leading IW function $\xi(\omega)$ or they are

zero. It is thus convenient to factor out the IW function and define $\hat{h}_i(\omega) = h_i(\omega)/\xi(\omega)$, which, up to $\mathcal{O}(\alpha_s, \Lambda_{\text{QCD}}/m_{c,b})$ corrections, read [33]

$$\begin{aligned}\hat{h}_V &= 1 + \hat{\alpha}_s C_{V_1} + \epsilon_c(\hat{L}_2 - \hat{L}_5) + \epsilon_b(\hat{L}_1 - \hat{L}_4), \\ \hat{h}_{A_1} &= 1 + \hat{\alpha}_s C_{A_1} + \epsilon_c\left(\hat{L}_2 - \hat{L}_5\frac{\omega-1}{\omega+1}\right) + \epsilon_b\left(\hat{L}_1 - \hat{L}_4\frac{\omega-1}{\omega+1}\right), \\ \hat{h}_{A_2} &= \hat{\alpha}_s C_{A_2} + \epsilon_c(\hat{L}_3 + \hat{L}_6), \\ \hat{h}_{A_3} &= 1 + \hat{\alpha}_s(C_{A_1} + C_{A_3}) + \epsilon_c(\hat{L}_2 - \hat{L}_3 + \hat{L}_6 - \hat{L}_5) + \epsilon_b(\hat{L}_1 - \hat{L}_4),\end{aligned}\tag{15}$$

$$\begin{aligned}\hat{h}_+ &= 1 + \hat{\alpha}_s\left[C_{V_1} + \frac{\omega+1}{2}(C_{V_2} + C_{V_3})\right] + (\epsilon_c + \epsilon_b)\hat{L}_1, \\ \hat{h}_- &= \hat{\alpha}_s\frac{\omega+1}{2}(C_{V_2} - C_{V_3}) + (\epsilon_c - \epsilon_b)\hat{L}_4.\end{aligned}\tag{16}$$

The terms proportional to $\hat{\alpha}_s = \alpha_s/\pi$ are perturbative corrections computed by matching QCD to the HQET and, although dependent on ω , are independent of the light degrees of freedom. The different $C_{A,V}$ functions can be found in Appendix A of Ref. [33]. In addition, $\epsilon_{c,b}$ are given by $\epsilon_{c,b} = \bar{\Lambda}/(2m_{c,b})$, with $\bar{\Lambda}$ a low energy constant (LEC) of order $\mathcal{O}(\Lambda_{\text{QCD}})$ for which we take the value quoted in Ref. [33]. The six ω -dependent \hat{L}_j functions can be written in terms of just three sub-leading IW functions $\hat{\chi}_{2,3}$ and η (see Eq. (8) in Ref. [33]) for which the near zero-recoil ($\omega = 1$) expansions²

$$\hat{\chi}_2(\omega) = \hat{\chi}_2(1) + \hat{\chi}'_2(1)(\omega - 1), \quad \hat{\chi}_3(\omega) = \hat{\chi}'_3(1)(\omega - 1), \quad \eta(\omega) = \eta(1) + \eta'(1)(\omega - 1)\tag{17}$$

are used. Strictly speaking, $\bar{\Lambda}$ depends on the light-quark degrees of freedom. Thus, one expects some SU(3) breaking that will modify its value compared to that used in Ref. [33] for $\bar{B} \rightarrow D^{(*)}$ decays. By keeping it the same, we reabsorb this change into the sub-leading IW functions which, together with the leading one, also suffer from SU(3) breaking effects.

For the leading IW function ξ we shall take the parametrization in Ref. [35], where one has that

$$\xi(\omega) = 1 - 8\rho^2\hat{z} + (64c - 16\rho^2)\hat{z}^2 + (256c - 24\rho^2 + 512d)\hat{z}^3\tag{18}$$

and

$$\hat{z}(\omega) = \frac{\sqrt{\omega+1} - \sqrt{2}}{\sqrt{\omega+1} + \sqrt{2}}.\tag{19}$$

In addition, following Ref. [35], we include the $\mathcal{O}[(\Lambda_{\text{QCD}}/m_c)^2]$ corrections introduced in Ref. [36], which affect the form factors that are protected from $\mathcal{O}(\Lambda_{\text{QCD}}/m_c)$ corrections at zero recoil, \hat{h}_+ and \hat{h}_{A_1} . We shall then use [36]

$$\hat{h}_+ \rightarrow \hat{h}_+ + \epsilon_c^2 l_1(1), \quad \hat{h}_{A_1} \rightarrow \hat{h}_{A_1} + \epsilon_c^2 l_2(1)\tag{20}$$

C. Fit of the SM-LQCD form factors to their HQSS/HQET expressions.

Treating the ten HQET LECs $\rho^2, c, d, \hat{\chi}_2(1), \hat{\chi}'_2(1), \hat{\chi}'_3(1), \eta(1), \eta'(1), l_1(1)$ and $l_2(1)$ introduced above as free parameters, we can fit the SM-LQCD form factors to their HQSS expressions. We

² In the case of $\hat{\chi}_3$ one has that $\hat{\chi}_3(1) = 0$ from Luke's theorem [34].

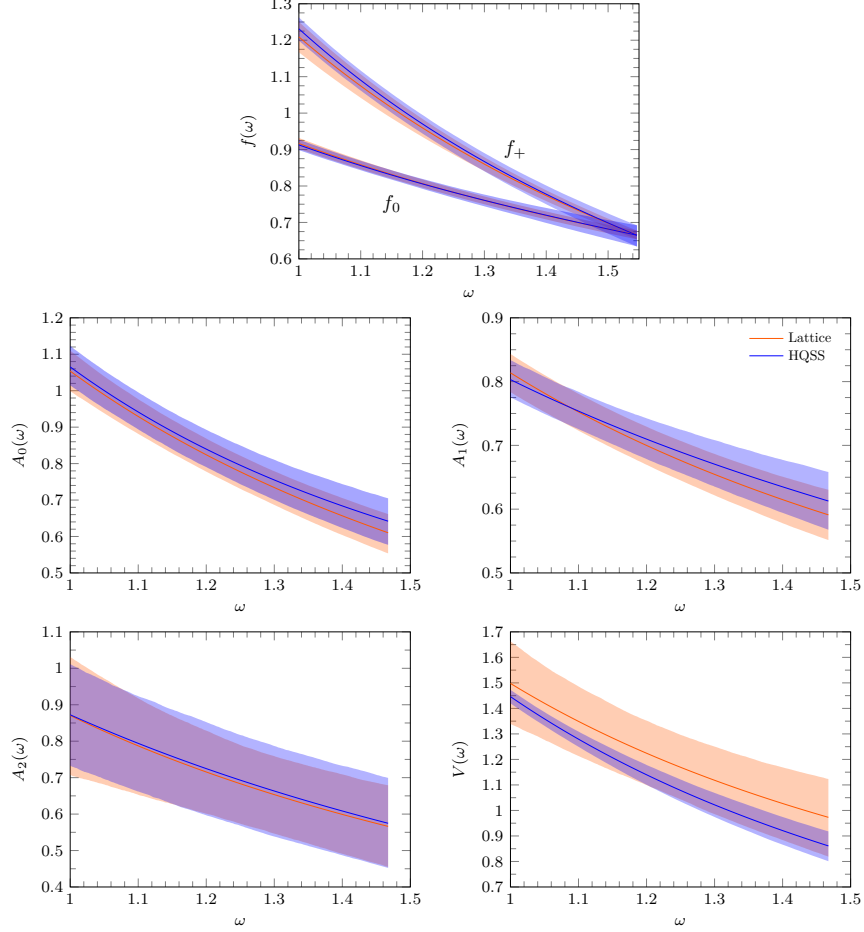


FIG. 2. Comparison of the original SM-LQCD form factors for $\bar{B}_s \rightarrow D_s$ [31] and $\bar{B}_s \rightarrow D_s^*$ [32] semileptonic decays and the HQET predictions after the fitting procedure described in the main text.

fit the twenty independent coefficients $a_i^{F=+,0,A_0,A_1,A_2,V}$ expressing SM-LQCD form factors. The fit minimizes a χ^2 function, that in a simplified notation we can write as

$$\chi^2 = \sum_j \sum_k (a_j - f_j) C_{jk}^{-1} (a_k - f_k). \quad (21)$$

Here, the sum is over all the expansion coefficients, for which the a 's represent their central values, and the f 's stand for the expressions of the corresponding expansion coefficients in terms of the ρ^2 , c , d , $\hat{\chi}_2(1)$, $\hat{\chi}'_2(1)$, $\hat{\chi}'_3(1)$, $\eta(1)$, $\eta'(1)$, $l_1(1)$ and $l_2(1)$ best fit LECs. The f_j terms are obtained by expanding each of the HQSS form factors, multiplied by the pole factors in the corresponding lattice form factors, in powers of the $z^*(z)$ variable for the $D_s^*(D_s)$ case. The covariance matrix C is block diagonal, built from the separate D_s^* and D_s covariances.

Since the SM-LQCD results come from simulations on the same ensembles, with the same lattice actions and the same treatment of the chiral and continuum limits, we expect correlations between as well as within them. Lacking information on the former, we also tried fits with the D_s^* results taken as either fully correlated or fully anti-correlated with the D_s ones. That is, we augmented the correlation matrix corresponding to C with off-diagonal blocks for these two extreme cases with all entries taken to be either 1 or -1 . However, the new C matrices constructed in this way had negative eigenvalues. We also explored partially correlated scenarios (all matrix elements of

	$\bar{B}_s \rightarrow D_s^{(*)}$	$\bar{B}_s \rightarrow D_s^{(*)}$ (unc)	$\epsilon[\bar{B}_s \rightarrow D_s^{(*)}]$	$\bar{B} \rightarrow D^{(*)}$ [35]
ρ^2	1.26 ± 0.07	1.33 ± 0.10	0.10	1.32 ± 0.06
c	1.20 ± 0.11	1.28 ± 0.13	0.13	1.20 ± 0.12
d	-0.91 ± 0.10	-0.97 ± 0.12	0.11	-0.84 ± 0.17
$\hat{\chi}_2(1)$	0.30 ± 0.23	0.18 ± 0.24	0.26	-0.058 ± 0.020
$\hat{\chi}'_2(1)$	0.14 ± 0.08	-0.02 ± 0.15	0.18	0.001 ± 0.020
$\hat{\chi}'_3(1)$	0.08 ± 0.09	0.07 ± 0.08	0.09	0.036 ± 0.020
$\eta(1)$	0.07 ± 0.21	0.14 ± 0.23	0.22	0.355 ± 0.040
$\eta'(1)$	-0.51 ± 0.25	0.12 ± 0.59	0.68	-0.03 ± 0.11
$l_1(1)$	0.28 ± 0.50	0.38 ± 0.52	0.51	0.14 ± 0.23
$l_2(1)$	-2.24 ± 0.94	-2.66 ± 1.1	1.03	-2.00 ± 0.30

TABLE I. Second column: Mean values and uncertainties of the $\rho^2, c, d, \hat{\chi}_2(1), \hat{\chi}'_2(1), \hat{\chi}'_3(1), \eta(1)$ and $\eta'(1)$ LECs obtained by fitting the $\bar{B}_s \rightarrow D_s^{(*)}$ SM-LQCD form factors from Refs. [31, 32] to their $\mathcal{O}(\alpha_s, \Lambda_{\text{QCD}}/m_{c,b})$ HQET expressions given in [33]. The first three parameters determine the leading IW function, while the last five enter in the $1/m_{c,b}$ sub-leading corrections. In addition, $l_1(1)$ and $l_2(1)$ account for $\mathcal{O}[(\Lambda_{\text{QCD}}/m_c)^2]$ contributions [36], which affect the \hat{h}_+ and \hat{h}_{A_1} form factors, respectively, which are protected from $\mathcal{O}(\Lambda_{\text{QCD}}/m_c)$ corrections at zero recoil. Third column: Results from the totally uncorrelated fit, where we consider only the diagonal elements of the matrix C in the definition of the merit function of Eq. (21). Fourth column: Final total errors considered on the fitted LECs and used in the evaluation of the uncertainty bands for derived observables. They are computed by combining in quadrature the errors from the central fit (second column) with the magnitudes of the differences between the mean values of the central and uncorrelated fits. Fifth column: Results for the analogous SU(3) fit carried out in Ref. [35] to $\bar{B} \rightarrow D^{(*)}$ form-factor LQCD and experimental inputs. Note a typo (global sign) in the numerical value of $l_2(1)$ given in the original Table 1 of Ref. [35].

ρ^2	c	d	$\hat{\chi}_2(1)$	$\hat{\chi}'_2(1)$	$\hat{\chi}'_3(1)$	$\eta(1)$	$\eta'(1)$	$l_1(1)$	$l_2(1)$
1.000	0.808	-0.709	0.207	-0.070	0.537	-0.003	0.124	-0.064	0.112
	1.000	-0.986	0.165	0.451	0.428	-0.072	0.207	-0.078	0.113
		1.000	-0.147	-0.544	-0.374	0.085	-0.210	0.075	-0.105
			1.000	0.049	0.901	-0.231	-0.213	-0.042	0.050
				1.000	-0.011	-0.176	-0.177	-0.005	0.075
					1.000	-0.030	-0.002	-0.091	-0.001
						1.000	0.344	0.226	-0.463
							1.000	-0.058	-0.183
								1.000	-0.107
									1.000

TABLE II. Correlation matrix of the $\rho^2, c, d, \hat{\chi}_2(1), \hat{\chi}'_2(1), \hat{\chi}'_3(1), \eta(1), \eta'(1), l_1(1)$ and $l_2(1)$ bestfit parameters after fitting the SM-LQCD form factors from Refs. [31, 32] to their $\mathcal{O}(\alpha_s, \Lambda_{\text{QCD}}/m_{c,b})$ HQET expressions.

the $D_s - D_s^*$ off-diagonal blocks set to r , with $|r| \leq 1$), but we found positive definite covariance matrices only for very small correlations $|r|$, of order a few percent. Finally, we carried out a totally uncorrelated fit, where we considered only the diagonal elements of the matrix C in the definition of the merit function of Eq. (21). That is to say, in this fit we also switched off the separate D_s^* and D_s correlations.

The results for the central fitted parameters and errors are given in the second column of Table I, while the corresponding correlation matrix appears in Table II. The fit has $\chi^2/\text{dof} = 0.81$. The next column shows the results from the totally uncorrelated fit (diagonal C matrix) which has

$\chi^2/\text{dof} = 0.29$. The two fits give compatible results, with parameter errors slightly larger for the latter. We take the magnitude of the differences between the mean values of the central fit and those obtained in the uncorrelated (diagonal C matrix) fit as a further systematic error that we will combine in quadrature with the errors from the central fit to get our final error estimate for each of the parameters. Their values are presented in the next-to-last column of Table I. We retain the correlation matrix from the central fit (Table II). Using these ingredients we construct Gaussian distributions which are then used to compute 68% confidence level bands for derived observables.

In the final column of Table I, we include Table 1 of [35], which contains the results for the analogous fit carried out in that work to $\bar{B} \rightarrow D^{(*)}$ LQCD and experimental form-factor inputs. We see in general small variations, compatible with the expected SU(3)-light flavor breaking corrections ($\sim 25 - 30\%$), except for some parameters, which control the sub-leading corrections and in most cases generate higher powers of $(\omega - 1)$, where the differences between the central values in both fits are bigger. However, these LECs are determined with sizable uncertainties, limiting an interpretation as possible unexpectedly large SU(3) breaking effects.

A comparison of the original SM-LQCD form factors from Refs. [31, 32] and the HQET predictions after the fitting procedure just described is shown in Fig. 2. There is a good agreement, within uncertainties, for all form-factors. Nevertheless, the HQET prediction for V is systematically below the LQCD result, with the uncertainty band of the former accommodated within the lower part of the error band of the latter (LQCD), which is notably much wider. We also observe some discrepancies between HQET and LQCD uncertainty bands for $f_+(\omega)$ close to zero recoil.

In the next subsection, we show the different q^2 -distributions that fully determine the semileptonic $\bar{B}_s \rightarrow D_s^{(*)} \tau^- \bar{\nu}_\tau$ transitions for polarized final tau-leptons [37, 38].

D. Visible kinematics of the sequential $H_b \rightarrow H_c \tau^- (\pi^- \nu_\tau, \rho^- \nu_\tau, \ell^- \bar{\nu}_\ell \nu_\tau) \bar{\nu}_\tau$ decays

If the spins of the $H_{b,c}$ hadrons are not measured, the ideal experiment to obtain the maximum information would be one in which both the momentum and spin (or helicity) state of the τ lepton could be established. This is however not possible since the τ is very short-lived. Thus, information about the $H_b \rightarrow H_c \tau^- \bar{\nu}_\tau$ parent decay has to be accessed via the visible kinematics of the τ decay products.

We have considered the three τ decay channels $\tau^- \rightarrow \pi^- \nu_\tau, \rho^- \nu_\tau$ and $\ell^- \bar{\nu}_\ell \nu_\tau$, with $\ell = \mu, e$, that account for up to 70% of the total τ decay width. Of the τ -decay products, only the charged particle $d = \pi^-, \rho^-$ or ℓ^- will be observed and, in the zero τ -width limit, one can write the differential decay width [38–41]

$$\frac{d^3\Gamma_d}{d\omega d\xi_d d\cos\theta_d} = \mathcal{B}_d \frac{d\Gamma_{\text{SL}}}{d\omega} \left\{ F_0^d(\omega, \xi_d) + F_1^d(\omega, \xi_d) \cos\theta_d + F_2^d(\omega, \xi_d) P_2(\cos\theta_d) \right\}. \quad (22)$$

As already mentioned, ω is the product of the four-velocities of the H_b and H_c hadrons, which is related to the four-momentum transfer squared q^2 through the relation $q^2 = M^2 + M'^2 - 2MM'$, with $M(M')$ the mass of the $H_b(H_c)$ hadron. In addition, ξ_d is the ratio of the d charged particle and τ energies measured in the $\tau^- \bar{\nu}_\tau$ center of mass frame (CM), while θ_d is the angle made by the three-momenta of the d charged particle and the H_c final hadron, also measured in the CM frame (for the kinematics, see for instance Fig. 1 of Ref. [42]). \mathcal{B}_d is the branching ratio for the corresponding τ decay mode and P_2 stands for the Legendre polynomial of order two. In addition, $d\Gamma_{\text{SL}}/d\omega$ accounts for the unpolarized $H_b \rightarrow H_c \tau^- \bar{\nu}_\tau$ decay width that can be written as [42]

$$\frac{d\Gamma_{\text{SL}}}{d\omega} = \frac{G_F^2 |V_{cb}|^2 M'^3 M^2}{24\pi^3} \sqrt{\omega^2 - 1} \left(1 - \frac{m_\tau^2}{q^2}\right)^2 n_0(\omega), \quad (23)$$

with G_F the Fermi decay constant and V_{cb} the corresponding Cabibbo-Kobayashi-Maskawa matrix element. The $n_0(\omega)$ function contains all the dynamical information, including possible NP effects. Finally, the $F_{0,1,2}^d(\omega, \xi_d)$ functions read [38]

$$\begin{aligned} F_0^d(\omega, \xi_d) &= C_n^d(\omega, \xi_d) + C_{P_L}^d(\omega, \xi_d) \langle P_L^{\text{CM}} \rangle(\omega), \\ F_1^d(\omega, \xi_d) &= C_{A_{FB}}^d(\omega, \xi_d) A_{FB}(\omega) + C_{Z_L}^d(\omega, \xi_d) Z_L(\omega) + C_{P_T}^d(\omega, \xi_d) \langle P_T^{\text{CM}} \rangle(\omega), \\ F_2^d(\omega, \xi_d) &= C_{A_Q}^d(\omega, \xi_d) A_Q(\omega) + C_{Z_Q}^d(\omega, \xi_d) Z_Q(\omega) + C_{Z_\perp}^d(\omega, \xi_d) Z_\perp(\omega). \end{aligned} \quad (24)$$

with $C_a^d(\omega, \xi_d)$ kinematical coefficients that are decay-mode dependent and whose expressions can be found in Appendix G of Ref. [38]. The rest of the observables in Eq. (24) represent spin ($\langle P_{L,T}^{\text{CM}} \rangle(\omega)$), angular ($A_{FB,Q}(\omega)$) and spin-angular ($Z_{L,Q,\perp}(\omega)$) asymmetries of the $H_b \rightarrow H_c \tau \bar{\nu}_\tau$ parent decay [38]. In the absence of CP-odd contributions, these asymmetries, together with $d\Gamma_{\text{SL}}/d\omega$, encode the maximal information obtainable if one could directly analyze the polarized $H_b \rightarrow H_c \tau \bar{\nu}_\tau$ transitions (see Ref. [37] and especially Eq. (3.46) of Ref. [38] and the related discussion). All the above observables ($n_0, \langle P_{L,T}^{\text{CM}} \rangle, A_{FB,Q}$ and $Z_{L,Q,\perp}$) are determined by the matrix elements of the $b \rightarrow c$ current between the initial (H_b) and final (H_c) hadrons. After summing over hadron polarizations the hadron contributions can be expressed in terms of Lorentz scalar structure functions, which depend on q^2 or equivalently on ω , the hadron masses and some Wilson coefficients if physics beyond the SM is considered. Lorentz, parity and time-reversal transformations of the hadron currents and states limit their number, as discussed in detail in Ref. [43]. The discussion of Subsec. 2.2 of Ref. [38] shows how to get the unpolarized $d\Gamma_{\text{SL}}/d\omega$ distribution and the tau spin, angular and spin-angular asymmetries in terms of general structure functions which can be obtained from the matrix elements of the relevant hadron operators. The matrix elements are in turn parametrized in terms of form-factors. The findings of Refs. [38, 43] are quite general and can be applied not only to the SM but also to any extension of the SM based on the low-energy effective Hamiltonian comprising the full set of dimension-6 semileptonic $b \rightarrow c \tau \bar{\nu}_\tau$ operators with left- and right-handed neutrino fields.

For pseudoscalar meson decay into pseudoscalar or vector mesons, the relations between structure functions and form-factors can be found in Appendix B of Ref. [44].

In Figs. 3 and 4 we show, for the $\bar{B}_s \rightarrow D_s^*$ and $\bar{B}_s \rightarrow D_s$ semileptonic decays respectively, the results for the $d\Gamma/dq^2$ differential decay width and the different asymmetries, introduced above, that can be obtained from the measurement of the visible kinematics of the charged τ -decay product. Only the differential $d\Gamma/dq^2$ distribution was shown in the original LQCD work of Ref. [31] for $\bar{B}_s \rightarrow D_s$, while for the vector meson decay mode $\bar{B}_s \rightarrow D_s^*$, the tau forward-backward angular A_{FB} and spin $\langle P_L^{\text{CM}} \rangle$ asymmetries were also presented in [32]. The rest of the observables are shown here for the very first time for the SM in Figs. 3 and 4 and for some extensions of the SM in the next section. As for Figs. 3 and 4, they have been evaluated both with the SM-LQCD form factors from Refs. [31, 32] and with the SM-HQET form factors obtained in Subsec. II C. The two results agree within uncertainties in all cases.

All this gives us confidence in the quality of the fitted HQET IW functions so that we can go a step further and use the relations in Ref. [33] to obtain in addition the HQSS scalar, pseudoscalar and tensor form factors of the two $\bar{B}_s \rightarrow D_s^{(*)}$ semileptonic transitions. Using the full set of HQSS form factors we can address, in the next section, the possibility of NP effects in these two decays.

III. NEW PHYSICS EFFECTS IN $\bar{B}_s \rightarrow D_s^{(*)} \tau^- \nu_\tau$ SEMILEPTONIC DECAYS

Following Ref. [45], to account for NP effects in a model independent way, we shall take a phenomenological effective field theory approach in which we consider all dimension-six $b \rightarrow c \tau \bar{\nu}_\tau$

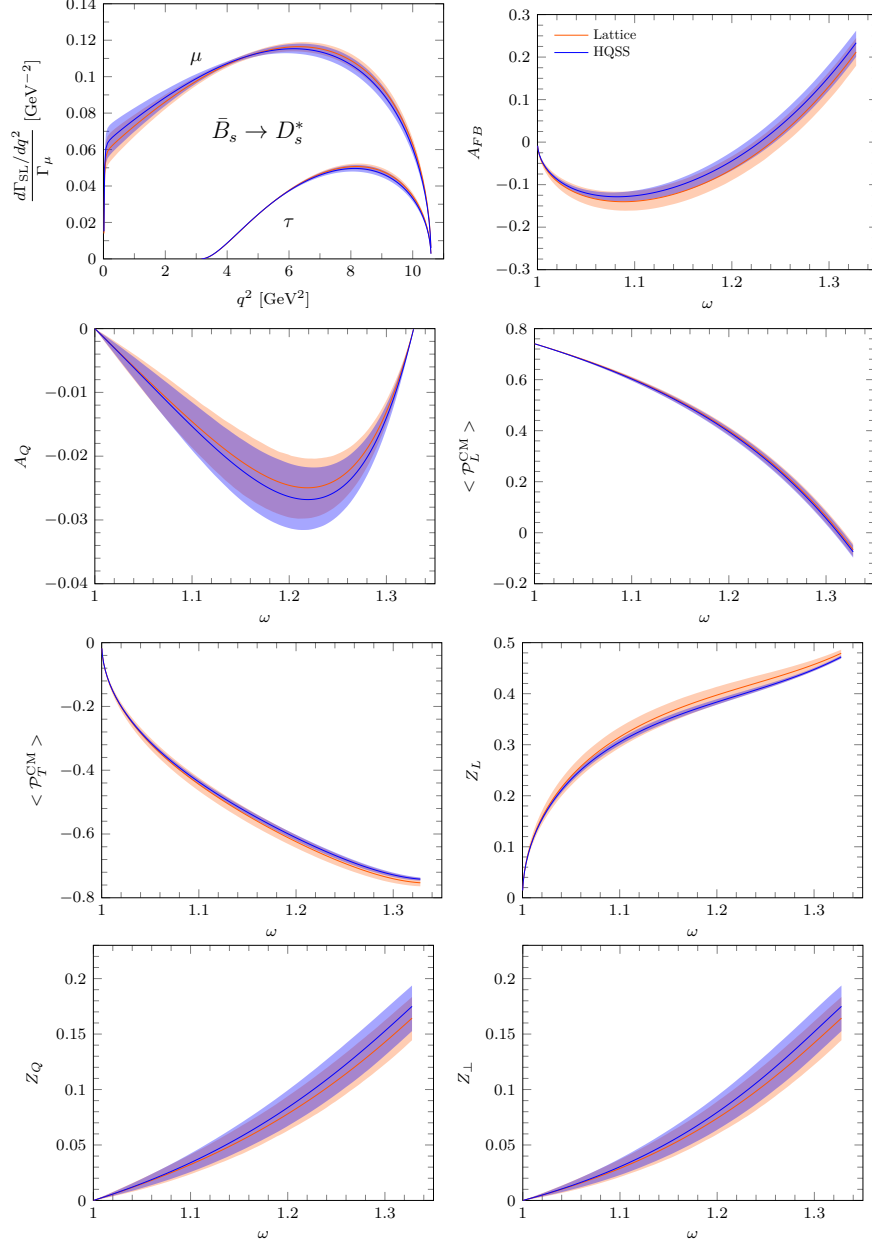


FIG. 3. $d\Gamma_{\text{SL}}/dq^2$ differential decay width, divided by $\Gamma_\mu = \Gamma(\bar{B}_s \rightarrow D_s^* \mu^- \bar{\nu}_\mu)$, and the different tau-asymmetries introduced in Eq. (24) for the semileptonic $\bar{B}_s \rightarrow D_s^* \tau^- \bar{\nu}_\tau$ decay. We compare the results evaluated with the SM-LQCD form factors from Refs. [31, 32] and with the SM-HQET form factors obtained after the fitting procedure described in Subsec. II C.

semileptonic operators (see Sec. III A below). These effective low energy operators are assumed to be generated by BSM physics that enters at a much higher energy scale. Their strengths are governed by Wilson coefficients (WCs) that can be fitted to experimental data. This data typically includes the $\mathcal{R}_{D^{(*)}} = \Gamma(B \rightarrow D^{(*)} \tau^- \bar{\nu}_\tau) / \Gamma(B \rightarrow D^{(*)} \mu^- \bar{\nu}_\mu)$ ratios, the tau longitudinal polarization asymmetry and the longitudinal D^* polarization (also measured by Belle [5, 46]), the τ forward-backward asymmetry and the upper bound for the $\bar{B}_c \rightarrow \tau \bar{\nu}_\tau$ decay rate [47]. There have been a large number of calculations along these lines, for the $\bar{B} \rightarrow D^{(*)}$ [33, 35, 37, 44, 45, 48–63],

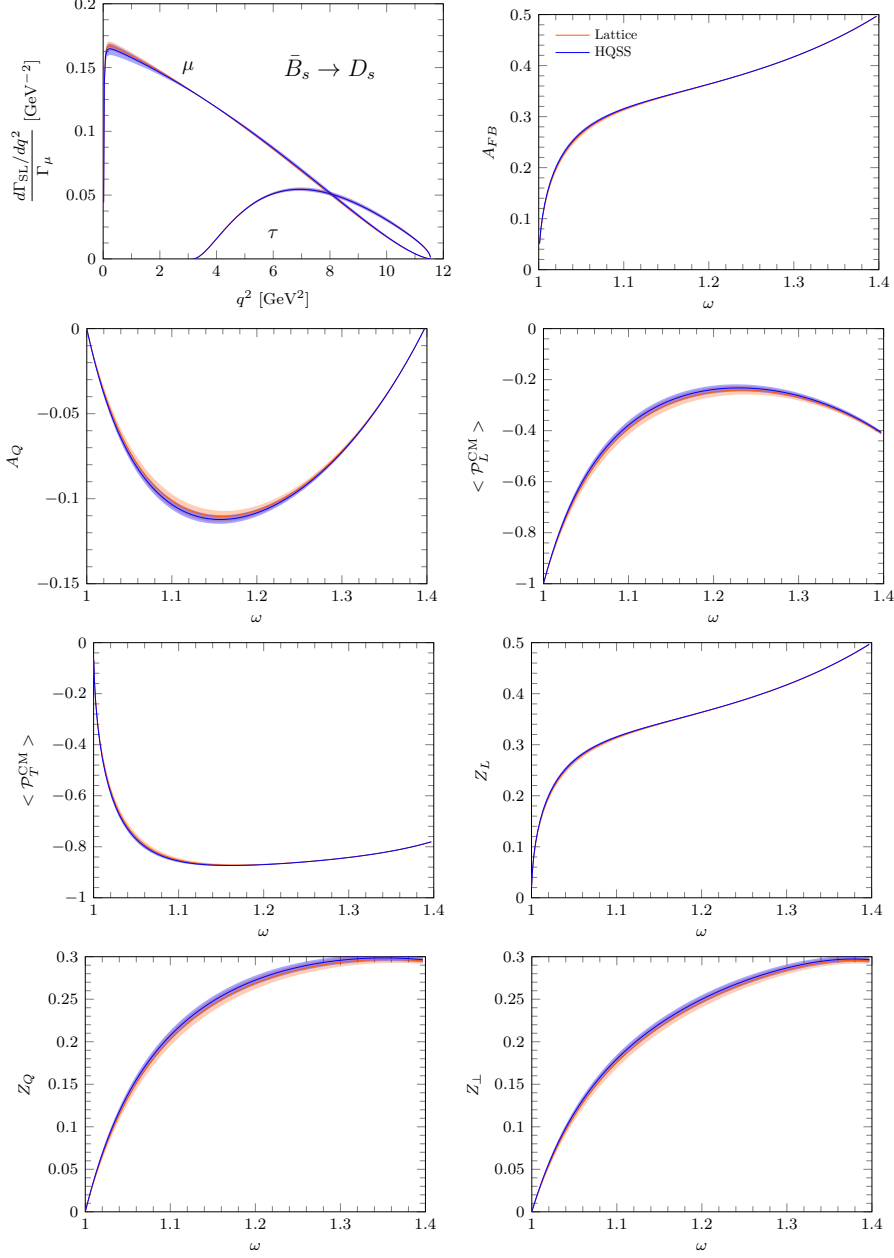


FIG. 4. Same as Fig. 3 for the $\bar{B}_s \rightarrow D_s$ semileptonic decay.

$\bar{B}_c \rightarrow J/\psi, \eta_c$ [22, 24, 44, 64, 65], $\Lambda_b \rightarrow \Lambda_c$ [35, 37, 43, 55, 66–79] and³ $\Lambda_b \rightarrow \Lambda_c(2595), \Lambda_c(2625)$ [71, 80, 81, 84–87] semileptonic decays.

Here, profiting from the lattice determination of the SM form factors in Refs. [31, 32] and the HQET study of $\bar{B} \rightarrow D^{(*)}$ form factors in Ref. [33], we have obtained all the $\bar{B}_s \rightarrow D_s^{(*)}$ form factors needed for a similar study of the $\bar{B}_s \rightarrow D_s^{(*)} \tau \bar{\nu}_\tau$ semileptonic decays. If NP is responsible for LFUV, one would expect to see its effects in these reactions at a level similar to that found in

³ The isoscalar $\Lambda_c(2595)$ and $\Lambda_c(2625)$, with $J^P = 1/2^-$ and $3/2^-$ respectively, are promising candidates for the lightest charmed baryon heavy-quark-spin doublet of odd parity resonances [80–82], although some reservations are given in [83]. Experimental distributions for the semileptonic decay of the ground-state bottom baryon Λ_b into both excited states would definitely help shed light on this issue [82].

the analogous $\bar{B} \rightarrow D^{(*)}$ decays. In addition to the $\mathcal{R}_{D_s^{(*)}} = \Gamma(\bar{B} \rightarrow D^{(*)s} \tau \bar{\nu}_\tau) / \Gamma(\bar{B}_s \rightarrow D_s^{(*)} \ell \bar{\nu}_\ell)$ ratios, we will investigate the role that the different asymmetries presented in Subsec. II D could play in establishing the presence of LFUV and, if experimentally confirmed, to distinguish between different extensions of the SM.

A. $H_b \rightarrow H_c \ell^- \bar{\nu}_\ell$ Effective Hamiltonian

The effective low-energy Hamiltonian that we use follows Ref. [60] and it includes all possible dimension-six semileptonic $b \rightarrow c$ operators with both left-handed (L) and right-handed (R) neutrino fields,

$$H_{\text{eff}} = \frac{4G_F V_{cb}}{\sqrt{2}} [(1 + C_{LL}^V) \mathcal{O}_{LL}^V + C_{RL}^V \mathcal{O}_{RL}^V + C_{LL}^S \mathcal{O}_{LL}^S + C_{RL}^S \mathcal{O}_{RL}^S + C_{LL}^T \mathcal{O}_{LL}^T + C_{LR}^V \mathcal{O}_{LR}^V + C_{RR}^V \mathcal{O}_{RR}^V + C_{LR}^S \mathcal{O}_{LR}^S + C_{RR}^S \mathcal{O}_{RR}^S + C_{RR}^T \mathcal{O}_{RR}^T] + h.c.. \quad (25)$$

Here, the C_{AB}^X ($X = S, V, T$ and $A, B = L, R$) are, complex in general, Wilson coefficients that parameterize the deviations from the SM. They can be lepton and flavor dependent although they are generally assumed to be nonzero only for the third quark and lepton generation. The dimension six operators read

$$\mathcal{O}_{(L,R)L}^V = (\bar{c} \gamma^\mu b_{L,R}) (\bar{\ell} \gamma_\mu \nu_{\ell L}), \quad \mathcal{O}_{(L,R)L}^S = (\bar{c} b_{L,R}) (\bar{\ell} \nu_{\ell L}), \quad \mathcal{O}_{LL}^T = (\bar{c} \sigma^{\mu\nu} b_L) (\bar{\ell} \sigma_{\mu\nu} \nu_{\ell L}), \quad (26)$$

$$\mathcal{O}_{(L,R)R}^V = (\bar{c} \gamma^\mu b_{L,R}) (\bar{\ell} \gamma_\mu \nu_{\ell R}), \quad \mathcal{O}_{(L,R)R}^S = (\bar{c} b_{L,R}) (\bar{\ell} \nu_{\ell R}), \quad \mathcal{O}_{RR}^T = (\bar{c} \sigma^{\mu\nu} b_R) (\bar{\ell} \sigma_{\mu\nu} \nu_{\ell R}), \quad (27)$$

with $\psi_{R,L} = (1 \pm \gamma_5) \psi / 2$. The effective Hamiltonian can be rewritten as [38]

$$H_{\text{eff}} = \frac{4G_F V_{cb}}{\sqrt{2}} \sum_{\chi=L,R} \left[\bar{c} (C_\chi^V \gamma^\mu + h_\chi C_\chi^A \gamma^\mu \gamma_5) b \bar{\ell} \gamma_\mu \nu_{\ell \chi} + \bar{c} (C_\chi^S + h_\chi C_\chi^P \gamma_5) b \bar{\ell} \gamma_\mu \nu_{\ell \chi} + C_\chi^T \bar{c} \sigma^{\mu\nu} (1 + h_\chi \gamma_5) b \bar{\ell} \sigma_{\mu\nu} \nu_{\ell \chi} \right] \quad (28)$$

with $h_L = -1, h_R = +1$ and

$$\begin{aligned} C_L^V &= (1 + C_{LL}^V + C_{RL}^V), & C_L^A &= (1 + C_{LL}^V - C_{RL}^V), \\ C_L^S &= (C_{LL}^S + C_{RL}^S), & C_L^P &= (C_{LL}^S - C_{RL}^S), & C_L^T &= C_{LL}^T, \\ C_R^V &= (C_{LR}^V + C_{RR}^V), & C_R^A &= -(C_{LR}^V - C_{RR}^V), \\ C_R^S &= (C_{LR}^S + C_{RR}^S), & C_R^P &= -(C_{LR}^S - C_{RR}^S), & C_R^T &= C_{RR}^T, \end{aligned} \quad (29)$$

We shall compare results obtained in the SM and in three different NP extensions. The latter correspond to the L Fit 7 of Ref [35], where only left-handed neutrino operators are considered, the R S7a scenario of Ref. [60] with only right-handed neutrino operators, and the left-handed neutrino L R_2 leptoquark model of Ref. [58], for which the two nonzero WCs (C_{LL}^S and C_{LL}^T) are complex⁴. In this latter case the effective Hamiltonian violates CP.

None of the observables $d\Gamma_{\text{SL}}/d\omega, \langle P_{L,T}^{\text{CM}} \rangle, A_{FB,Q}$ and $Z_{L,Q,\perp}$ entering Eqs. (22) and (24) are sensitive to CP-symmetry breaking terms [37, 38]. Hence, we will also show results for the L R_2 leptoquark model of Ref. [58] for other distributions, related to the tau polarization component (P_{TT}) along an axis perpendicular to the hadron-tau plane [37], which could be accessed if one could further measure the azimuthal angle (ϕ_d) of the charged d particle (see Fig. 1 of Ref. [42]).

⁴ The numerical values that we use for these two WCs can be found at the beginning of Subsec. 4.2.1 of Ref. [37].

Note that in the differential distribution given in Eq. (22) this angle has been integrated out since measuring ϕ_d would require full reconstruction of the tau three-momentum. The latter can be circumvented through the analysis of distributions that also involve the decay products of the H_c hadron. Thus, some CP-odd observables have been presented for $\bar{B} \rightarrow D^*$ and $\Lambda_b \rightarrow \Lambda_c$ decays in Refs. [50, 51, 53, 63] and Refs. [75, 77] respectively.

As already mentioned, we refer the reader to Ref. [38], and references therein, for a full account of our formalism.

B. Partially integrated sequential $H_b \rightarrow H_c \tau^- (\pi^- \nu_\tau, \rho^- \nu_\tau, \ell^- \bar{\nu}_\ell \nu_\tau) \bar{\nu}_\tau$ decay distributions

The feasibility of NP studies can be severely limited, however, by the statistical precision in the measurement of the triple differential decay width of Eq. (22). One can increase statistics, at the price of losing information in some of the observables, by integrating over one or more of the ω, ξ_d and θ_d variables, although in this case not all observables entering in Eq. (24) can be extracted. In this way one can obtain the distributions [42]

$$\frac{d^2\Gamma_d}{d\omega d\xi_d} = 2\mathcal{B}_d \frac{d\Gamma_{\text{SL}}}{d\omega} \left\{ C_n^d(\omega, \xi_d) + C_{P_L}^d(\omega, \xi_d) \langle P_L^{\text{CM}} \rangle(\omega) \right\}, \quad (30)$$

from which only $d\Gamma_{\text{SL}}/d\omega$ and the CM τ longitudinal polarization can be extracted, or

$$\frac{d^2\Gamma_d}{d\omega d\cos\theta_d} = \mathcal{B}_d \frac{d\Gamma_{\text{SL}}}{d\omega} \left[\frac{1}{2} + \tilde{F}_1^d(\omega) \cos\theta_d + \tilde{F}_2^d(\omega) P_2(\cos\theta_d) \right], \quad (31)$$

with

$$\tilde{F}_1^d(\omega) = C_{A_{FB}}^d(\omega) A_{FB}(\omega) + C_{Z_L}^d(\omega) Z_L(\omega) + C_{P_T}^d(\omega) \langle P_T^{\text{CM}} \rangle(\omega), \quad (32)$$

$$\tilde{F}_2^d(\omega) = C_{A_Q}^d(\omega) A_Q(\omega) + C_{Z_Q}^d(\omega) Z_Q(\omega) + C_{Z_\perp}^d(\omega) Z_\perp(\omega), \quad (33)$$

which retains information on $d\Gamma_{\text{SL}}/dq^2$ and six out of the seven original asymmetries. The latter cannot, however, be extracted from knowledge of \tilde{F}_1^d and \tilde{F}_2^d alone.

One can further integrate over ω to obtain [42]

$$\frac{d\Gamma_d}{d\cos\theta_d} = \mathcal{B}_d \Gamma_{\text{SL}} \left[\frac{1}{2} + \hat{F}_1^d \cos\theta_d + \hat{F}_2^d P_2(\cos\theta_d) \right], \quad \hat{F}_{1,2}^d = \frac{1}{\Gamma_{\text{SL}}} \int_1^{\omega_{\text{max}}} \frac{d\Gamma_{\text{SL}}}{d\omega} \tilde{F}_{1,2}^d(\omega) d\omega. \quad (34)$$

and

$$\frac{d\Gamma_d}{dE_d} = 2\mathcal{B}_d \int_{\omega_{\text{inf}}(E_d)}^{\omega_{\text{sup}}(E_d)} d\omega \frac{1}{\gamma m_\tau} \frac{d\Gamma_{\text{SL}}}{d\omega} \left\{ C_n^d(\omega, \xi_d) + C_{P_L}^d(\omega, \xi_d) \langle P_L^{\text{CM}} \rangle(\omega) \right\}, \quad (35)$$

where $\gamma = (q^2 + m_\tau^2)/(2m_\tau \sqrt{q^2})$ and, in the latter case, the appropriate ω limits can be found in Ref. [42].

Although the information on the individual asymmetries is now completely lost, the above two distributions could still be useful observables in the search for NP beyond the SM.

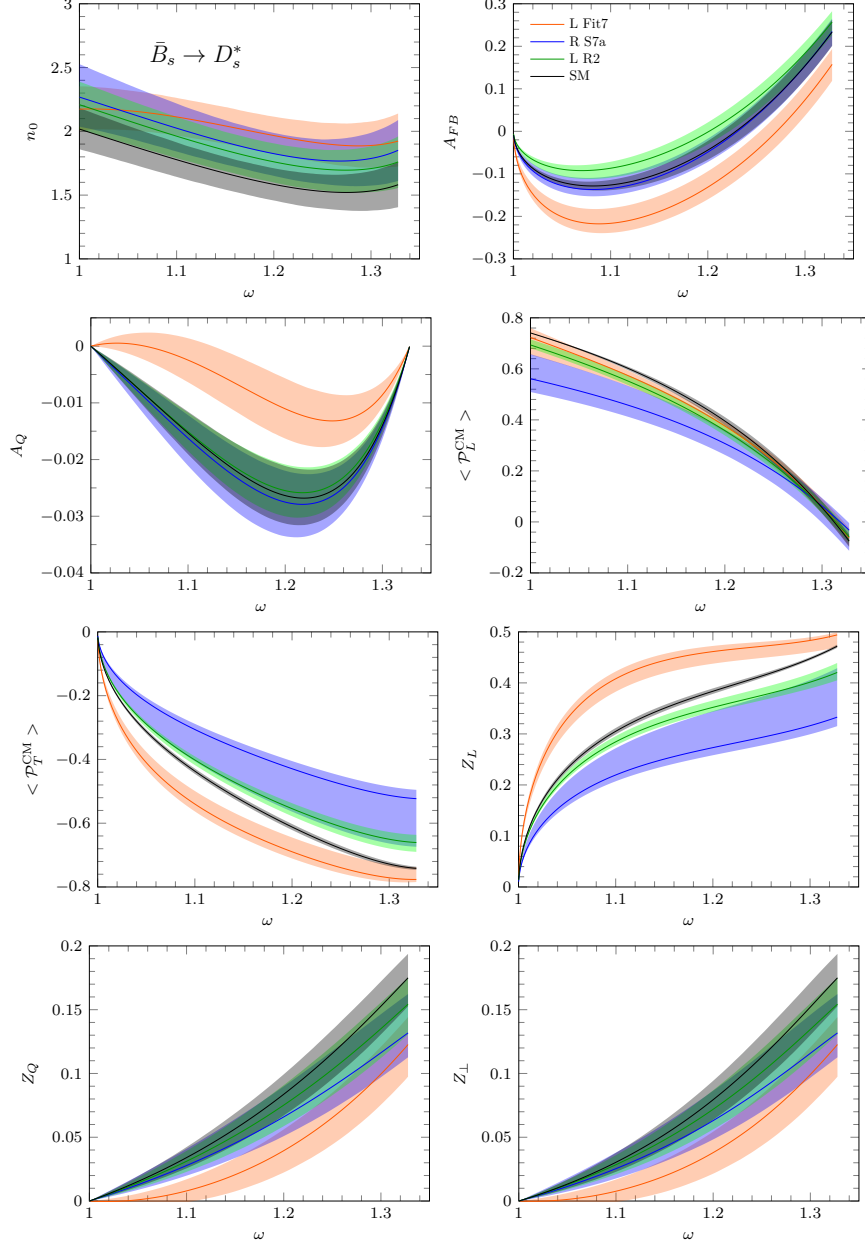


FIG. 5. Distribution n_0 from Eq. (23) and the tau asymmetries introduced in Eq. (24) for the $\bar{B}_s \rightarrow D_s^* \tau \bar{\nu}_\tau$ decay. We compare the results for these observables obtained in the SM and the NP models L Fit 7, R S7a and L R_2 of Refs [35], [60] and [58], respectively. We use the HQET form-factors derived from the SM-LQCD form factors obtained in Refs. [31, 32].

C. NP results and discussion

1. LFUV ratios, unpolarized differential decay widths and tau angular, spin and spin-angular asymmetries

We start by showing, in Table III, the values for the semileptonic decay widths $\Gamma_\tau = \Gamma(\bar{B}_s \rightarrow D_s^{(*)} \tau \bar{\nu}_\tau)$ and $\Gamma_\ell = \Gamma(\bar{B}_s \rightarrow D_s^{(*)} \ell \bar{\nu}_\ell)$, with $\ell = e, \mu$, and the corresponding $\mathcal{R}_{D_s^{(*)}}$ ratios, evaluated within the SM and the three NP extensions, L Fit 7 of Ref [35], R S7a scenario of Ref. [60] and the

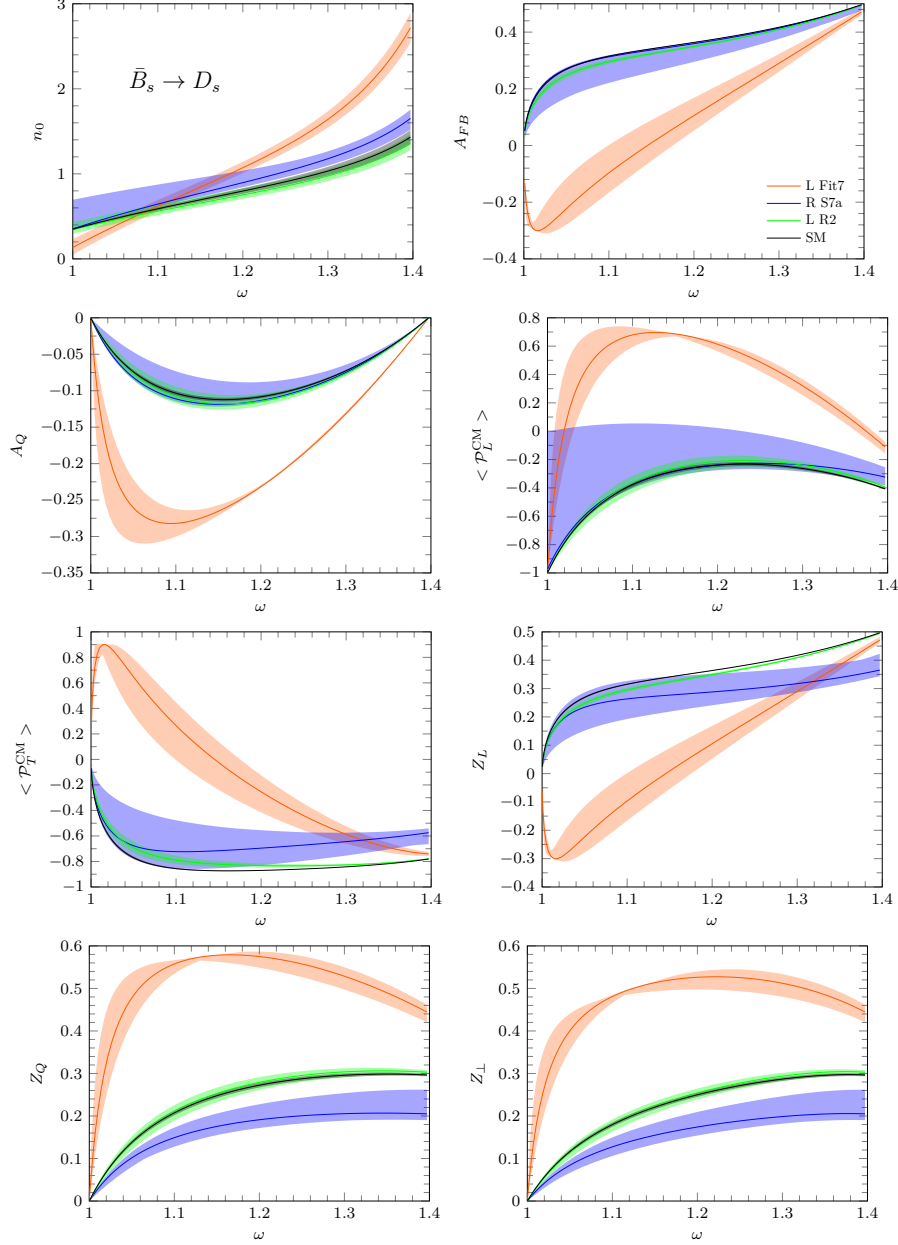


FIG. 6. Same as Fig. 5 but for the $\bar{B}_s \rightarrow D_s \tau \bar{\nu}_\tau$ transition.

L R_2 leptoquark model of Ref. [58], considered in this study. For the first two NP models, we see the ratios clearly deviate from the SM prediction⁵. Their central values are higher than SM ones, with the highest one corresponding always to L Fit 7, which leads to ratios around 5σ above the SM predictions. The results are similar to those obtained in Ref. [42] for the analogous $\bar{B} \rightarrow D^{(*)}$ decays (see Table 3 of that reference). In the L R_2 case, $\mathcal{R}_{D_s^*}$ is larger than the SM value while \mathcal{R}_{D_s} is lower and compatible within errors.

In Figs. 5 and 6 we show now the values for the $n_0(\omega)$ function introduced in Eq. (23), which

⁵ The LQCD results in Refs. [31] and [32] are $\mathcal{R}_{D_s}^{\text{SM}} = 0.2993(46)$ and $\mathcal{R}_{D_s^*}^{\text{SM}} = 0.2490(60)(35)$. The former is in excellent agreement with the prediction quoted in Table III obtained with the HQET parameterization of the $\bar{B}_s \rightarrow D_s$ form-factors. For $\mathcal{R}_{D_s^*}^{\text{SM}}$, we get a value around 0.6σ ($\sim 1.5\%$) smaller than quoted in [31].

		SM	L Fit 7 [35]	R S7a [60]	L R_2 [58]
$\bar{B}_s \rightarrow D_s$	$\Gamma_{e(\mu)}$	0.92 ± 0.06			
	Γ_τ	0.27 ± 0.01	0.36 ± 0.02	$0.305^{+0.061}_{-0.017}$	$0.259^{+0.029}_{-0.017}$
	\mathcal{R}_{D_s}	$0.298^{+0.009}_{-0.007}$	$0.391^{+0.021}_{-0.017}$	$0.333^{+0.066}_{-0.016}$	$0.283^{+0.031}_{-0.017}$
$\bar{B}_s \rightarrow D_s^*$	$\Gamma_{e(\mu)}$	$2.11^{+0.17}_{-0.22}$			
	Γ_τ	$0.52^{+0.04}_{-0.05}$	0.62 ± 0.05	0.59 ± 0.06	0.57 ± 0.05
	$\mathcal{R}_{D_s^*}$	$0.245^{+0.007}_{-0.006}$	$0.293^{+0.011}_{-0.007}$	$0.280^{+0.016}_{-0.015}$	0.27 ± 0.01

TABLE III. Semileptonic decay widths $\Gamma_\tau = \Gamma(\bar{B}_s \rightarrow D_s^{(*)} \tau \bar{\nu}_\tau)$ and $\Gamma_{e(\mu)} = \Gamma[\bar{B}_s \rightarrow D_s^{(*)} e(\mu) \bar{\nu}_{e(\mu)}]$ (in units of $10 \times |V_{cb}|^2 \text{ps}^{-1}$) and ratios $\mathcal{R}_{D_s^{(*)}} = \Gamma(\bar{B}_s \rightarrow D_s^{(*)} \tau \bar{\nu}_\tau) / \Gamma[\bar{B}_s \rightarrow D_s^{(*)} e(\mu) \bar{\nu}_{e(\mu)}]$ obtained using the SM-HQSS form factors, the NP model L Fit 7 (R S7a) of Ref [35] ([60]), which only includes left- (right-)handed neutrino NP operators and the L R_2 leptoquark model of Ref. [58]. Errors induced by the uncertainties in the form-factors and Wilson coefficients are added in quadrature.

contains all the dynamical information of the $d\Gamma_{\text{SL}}/d\omega$ differential decay width, and the set of tau spin, angular and spin-angular asymmetries introduced in Eq. (24). Most of the observables allow for a clear distinction between SM and L Fit 7 results, the exception being the CM longitudinal spin asymmetry $\langle P_L^{\text{CM}} \rangle$ for the $\bar{B}_s \rightarrow D_s^*$ decay. In fact, these observables also differentiate between L Fit 7 and the other two NP scenarios. With few exceptions, notably the Z_Q and Z_\perp asymmetries for the $\bar{B}_s \rightarrow D_s$ decays, the R S7a and L R_2 NP scenarios tend to agree within errors and they are closer to the SM, especially in the case of the L R_2 model.

As already mentioned, none of the observables shown so far is sensitive to CP breaking terms. To measure those one needs to analyze the CP violating triple product asymmetries that involve the decay of the H_c hadron [50, 51, 53, 63, 75, 77], or otherwise to be able to fully establish the tau three-momentum. In the latter case, one has access to the $\langle P_{TT}^{\text{CM}} \rangle(\omega)$ observable, which gives the component of the CM tau-polarization vector along an axis perpendicular to the hadron-tau plane (see Eqs. (3.14), (3.24) and (3.25) of Ref. [37]). Among the different NP extensions considered in this work, only the L R_2 leptoquark model of Ref. [58], with complex Wilson coefficients, can generate a nonzero value for the $\langle P_{TT}^{\text{CM}} \rangle(\omega)$ distribution. In this NP model, the two nonzero WCs C_{LL}^S and C_{LL}^T are given, at the bottom-mass scale appropriate for the present calculation, in terms of just the value of C_{LL}^T at the 1 TeV scale, where $C_{LL}^S(1 \text{ TeV}) = 4C_{LL}^T(1 \text{ TeV})$, and the corresponding evolution matrix (see Ref. [58]). The best fit of the WCs to the \bar{B} -meson LFUV signatures does not fix the sign of the imaginary part of $C_{LL}^T(1 \text{ TeV})$. Contrary to the other observables considered so far, $\langle P_{TT}^{\text{CM}} \rangle(\omega)$ is linear in this imaginary part and thus its measurement would break this degeneracy. The results for $\langle P_{TT}^{\text{CM}} \rangle(\omega)$, using both possible signs for $\text{Im}[C_{LL}^T(1 \text{ TeV})]$, are shown in the upper panels of Fig. 7 for the $\bar{B}_s \rightarrow D_s^*$ (left) and $\bar{B}_s \rightarrow D_s$ (right) decays respectively. We see that the absolute value of this distribution is around one order of magnitude larger for the pseudoscalar than for the vector decay modes. An observation of a nonzero $\langle P_{TT}^{\text{CM}} \rangle(\omega)$ value will be a clear indication of the existence of NP beyond the SM and CP violation.

In the bottom panel of Fig. 7 we show the degree of polarization of the tau

$$\langle P^2 \rangle(\omega) = -\langle P_L^2 + P_T^2 + P_{TT}^2 \rangle(\omega) \quad (36)$$

which is a Lorentz invariant quantity. As shown in Ref. [37], this is exactly -1 for $0^- \rightarrow 0^-$ transitions, reflecting the fact that for such decays the outgoing taus are fully polarized. Thus we only present the results for the $\bar{B}_s \rightarrow D_s^*$ decay. As seen from the figure this observable, which is sensitive to CP-odd terms in the effective Hamiltonian, discriminates very efficiently between

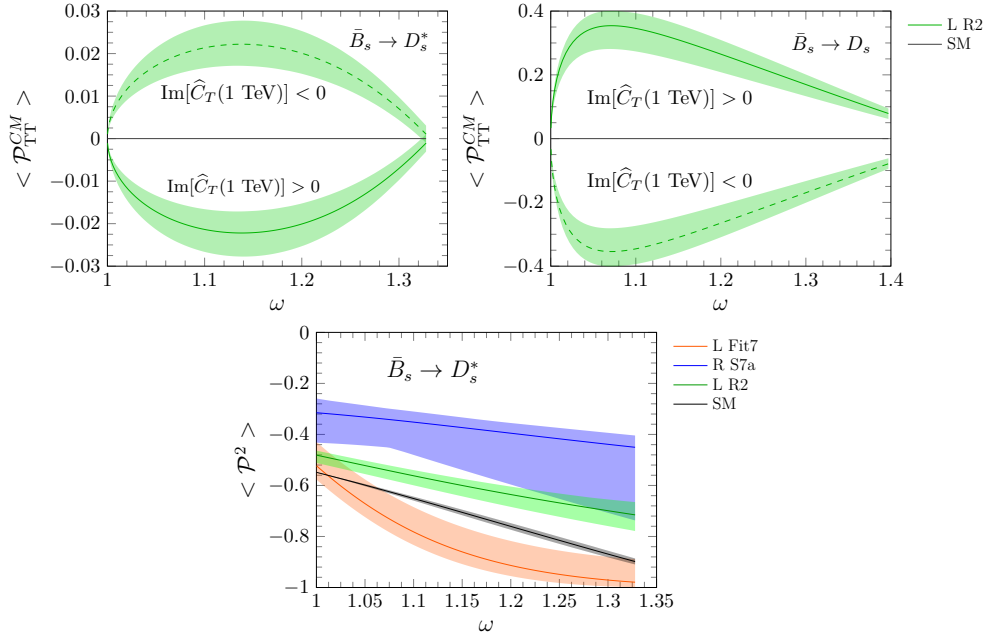


FIG. 7. Upper panels: $\langle P_{TT}^{CM} \rangle(\omega)$ for the $\bar{B}_s \rightarrow D_s^*$ (left) and $\bar{B}_s \rightarrow D_s$ (right) decays evaluated with the L R_2 leptoquark model of Ref. [58]. Bottom panel: comparison of the $\langle P^2 \rangle(\omega)$ distribution obtained in the SM and the NP extensions L Fit 7 [35], R S7a [60] and L R_2 [58].

different NP models and the SM.

2. Distributions of charged tau decay products

In Figs. 8 and 9, we give the products $n_0(\omega)\tilde{F}_{1,2}^d(\omega)$ (Eqs. (32) and (33)) that can be obtained from the measurement of the double differential decay width $d\Gamma_d/(d\omega d\cos\theta_d)$ corresponding to the $\bar{B}_s \rightarrow D_s^{(*)}\tau^-(\pi^-\nu_\tau, \rho^-\nu_\tau, \mu^-\bar{\nu}_\mu\nu_\tau)\bar{\nu}_\tau$ sequential decays⁶. In most cases, with the main exception being the $\tau \rightarrow \rho\nu_\tau$ decay mode for the $\bar{B}_s \rightarrow D_s^*$ decay, the predictions from the L Fit 7 model are clearly distinguishable from the ones obtained in the SM and the other two NP scenarios. The SM and the latter two NP models give results that agree within errors.

A similar situation is seen in Fig. 10, where we display the normalized $[\mathcal{B}_d\Gamma_{\text{SL}}]^{-1}d\Gamma_d/d\cos\theta_d$ angular distribution for the $\bar{B}_s \rightarrow D_s^{(*)}\tau^-(\pi^-\nu_\tau, \rho^-\nu_\tau, \mu^-\bar{\nu}_\mu\nu_\tau)\bar{\nu}_\tau$ sequential decays. Again, with the exception of the ρ channel for the $\bar{B}_s \rightarrow D_s^*$ decay, we see that the L Fit 7 NP scenario of Ref. [35] can be distinguished from the SM and the other two NP scenarios. This is most clearly seen for forward and backward angles of the pion and rho mesons from the hadronic τ -decay modes in the parent $\bar{B}_s \rightarrow D_s$ semileptonic decay. As for the R S7a scenario of Ref. [60] and L R_2 Fit of Ref. [58], their corresponding distributions are compatible with the SM and among themselves within errors. In fact, for the L R_2 model, the central values are very close to the SM ones. These behaviors derive from the ones seen for $\tilde{F}_{1,2}^d(\omega)$ in Figs. 8 and 9 and they are also seen in the corresponding $\hat{F}_{1,2}^d$ coefficients that we give in Tables IV and V for the leptonic and two hadronic τ -decay channels, respectively. These latter coefficients are obtained after integrating over ω the $\tilde{F}_{1,2}^d(\omega)$ functions, as indicated in Eq. (34), and depend on the tau-decay mode. For L Fit 7, we

⁶ The spin analyzing power makes the pion tau-decay mode a better candidate than the leptonic or rho modes for the extraction of information on the spin and spin-angular asymmetries (see discussion of Eq. (2.11) of Ref. [42]).

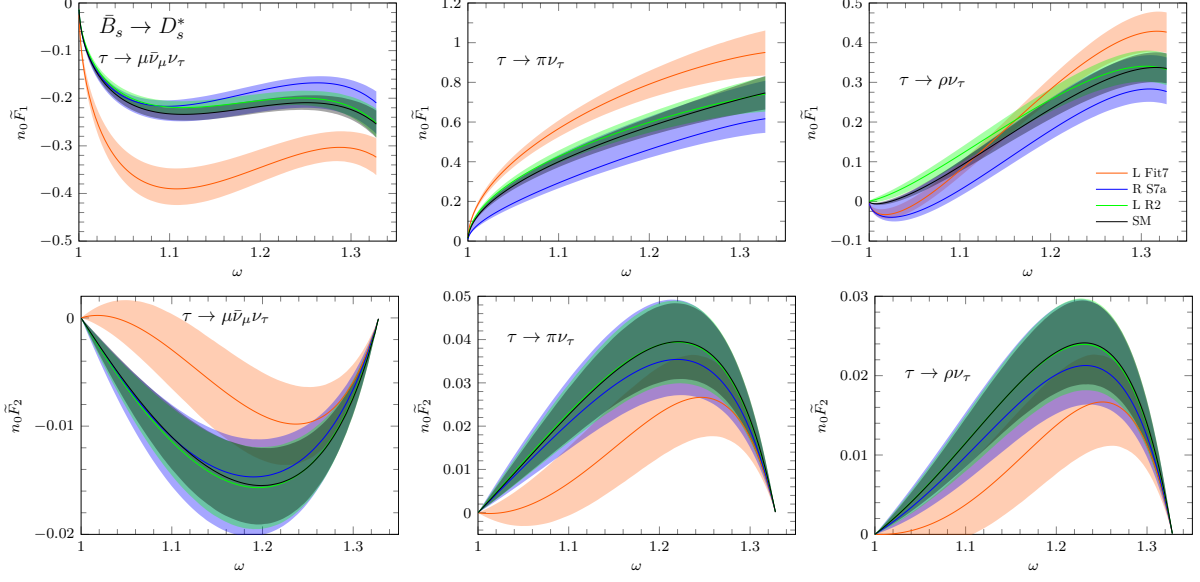


FIG. 8. Distributions $[n_0 \tilde{F}_1^d](\omega)$ and $[n_0 \tilde{F}_2^d](\omega)$ obtained from $d\Gamma_d/(d\omega d\cos\theta_d)$ (Eq. (31)) for the tau hadronic and leptonic $\bar{B}_s \rightarrow D_s^* \tau^- (\pi^- \nu_\tau, \rho^- \nu_\tau, \mu^- \bar{\nu}_\mu \nu_\tau) \bar{\nu}_\tau$ sequential decays.

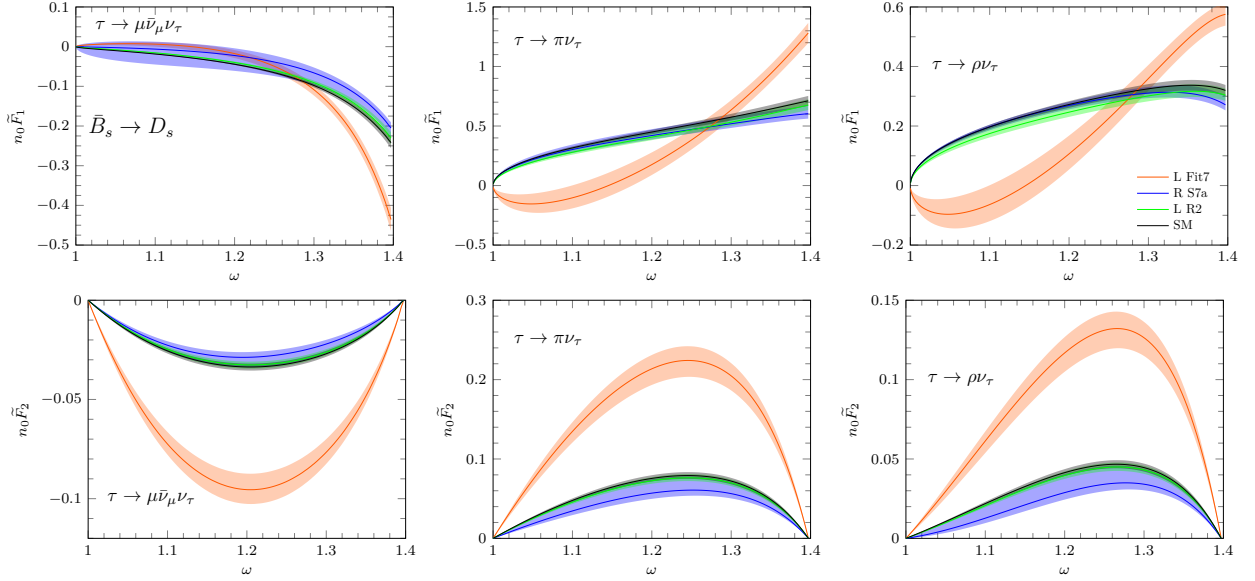


FIG. 9. Same as Fig. 8 for the $\bar{B}_s \rightarrow D_s \tau^- (\pi^- \nu_\tau, \rho^- \nu_\tau, \mu^- \bar{\nu}_\mu \nu_\tau) \bar{\nu}_\tau$ sequential decays.

generally find that one of the two coefficients is very different from SM and other NP model values. For the R S7a scenario, they are compatible with SM, within errors, and they are very close to the SM ones in the L R₂ case.

Finally, in Fig 11, we present the results for the dimensionless distribution

$$\hat{F}_0^d(E_d) = \frac{m_\tau}{2\mathcal{B}_d \Gamma_{\text{SL}}} \frac{d\Gamma_d}{dE_d}, \quad (37)$$

which contains all the relevant information on the $d\Gamma_d/dE_d$ energy differential decay width. For

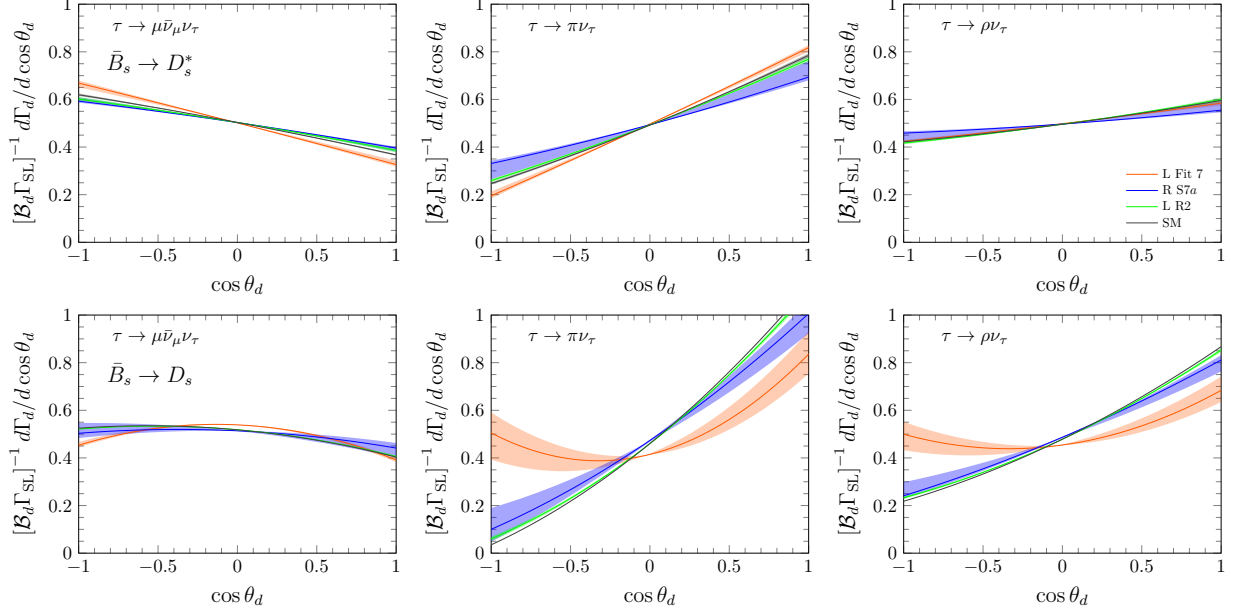


FIG. 10. The ω -integrated $d\Gamma_d/d\cos\theta_d$ distributions for the $\bar{B}_s \rightarrow D_s^* \tau^- (\pi^- \nu_\tau, \rho^- \nu_\tau, \mu^- \bar{\nu}_\mu \nu_\tau) \bar{\nu}_\tau$ (top) and $\bar{B}_s \rightarrow D_s \tau^- (\pi^- \nu_\tau, \rho^- \nu_\tau, \mu^- \bar{\nu}_\mu \nu_\tau) \bar{\nu}_\tau$ (bottom) sequential decays. Units of $[\mathcal{B}_d \Gamma_{\text{SL}}]^{-1}$.

		\widehat{F}_1^μ	\widehat{F}_2^μ
$\bar{B}_s \rightarrow D_s$	SM	$-0.0607^{+0.0004}_{-0.0003}$	-0.0359 ± 0.0008
	L fit 7	$-0.031^{+0.008}_{-0.011}$	$-0.0776^{+0.0023}_{-0.0005}$
	R fit S7a	$-0.03^{+0.02}_{-0.04}$	-0.028 ± 0.003
	L R_2	$-0.0579^{+0.0028}_{-0.0020}$	$-0.0367^{+0.0028}_{-0.0019}$
$\bar{B}_s \rightarrow D_s^*$	SM	-0.126 ± 0.004	-0.0068 ± 0.0014
	L Fit 7	$-0.171^{+0.017}_{-0.010}$	$-0.0025^{+0.0015}_{-0.0016}$
	R S7a	$-0.099^{+0.006}_{-0.016}$	$-0.0057^{+0.0014}_{-0.0022}$
	L R_2	$-0.108^{+0.006}_{-0.009}$	-0.0062 ± 0.0014

TABLE IV. Predictions for the angular moments $\widehat{F}_{1,2}^\mu$ for the $\bar{B}_s \rightarrow D_s^{(*)} \tau (\mu \bar{\nu}_\mu \nu_\tau) \bar{\nu}_\tau$ sequential decay evaluated in the SM and the same NP scenarios considered in Table III.

all three tau-decay channels considered. It is normalized as

$$\frac{1}{m_\tau} \int_{E_d^{\min}}^{E_d^{\min}} dE_d \widehat{F}_0^d(E_d) = \frac{1}{2}, \quad (38)$$

but its energy dependence is still affected by the CM τ longitudinal polarization $\langle P_L^{\text{CM}} \rangle(\omega)$. However, as seen in Fig 11, for the $\bar{B}_s \rightarrow D_s^*$ parent decay, all NP scenarios considered are compatible with SM predictions, and among themselves, within uncertainties, while for the $\bar{B}_s \rightarrow D_s$, the distribution obtained from the L Fit 7 NP model of Ref. [35] can be distinguished from all other predictions.

		\widehat{F}_1^π	\widehat{F}_2^π	\widehat{F}_1^ρ	\widehat{F}_2^ρ
$\bar{B}_s \rightarrow D_s$	SM	$0.5440^{+0.0017}_{-0.0020}$	$0.0791^{+0.0017}_{-0.0019}$	$0.3246^{+0.0010}_{-0.0012}$	$0.0426^{+0.0009}_{-0.0010}$
	L fit 7	$0.17^{+0.10}_{-0.08}$	$0.170^{+0.002}_{-0.008}$	$0.09^{+0.06}_{-0.05}$	$0.0916^{+0.0017}_{-0.0048}$
	R fit S7a	$0.45^{+0.05}_{-0.09}$	$0.053^{+0.012}_{-0.007}$	$0.285^{+0.015}_{-0.053}$	$0.026^{+0.008}_{-0.004}$
	L R_2	$0.520^{+0.010}_{-0.012}$	$0.080^{+0.004}_{-0.005}$	0.310 ± 0.006	$0.0430^{+0.0019}_{-0.0027}$
$\bar{B}_s \rightarrow D_s^*$	SM	0.269 ± 0.007	0.016 ± 0.003	$0.087^{+0.006}_{-0.007}$	0.0088 ± 0.0018
	L fit 7	$0.311^{+0.010}_{-0.017}$	0.006 ± 0.004	0.081 ± 0.007	0.0038 ± 0.0022
	R fit S7a	$0.182^{+0.067}_{-0.013}$	$0.012^{+0.005}_{-0.003}$	$0.048^{+0.035}_{-0.008}$	$0.0067^{+0.0031}_{-0.0018}$
	L R_2	$0.255^{+0.009}_{-0.008}$	0.014 ± 0.003	$0.091^{+0.006}_{-0.008}$	$0.0080^{+0.0019}_{-0.0020}$

TABLE V. Predictions for the angular moments $\widehat{F}_{1,2}^{\pi,\rho}$ for the $\bar{B}_s \rightarrow D_s^{(*)} \tau(\pi\nu_\tau, \rho\nu_\tau)\bar{\nu}_\tau$ sequential decays evaluated in the SM and the same NP scenarios considered in Table III.

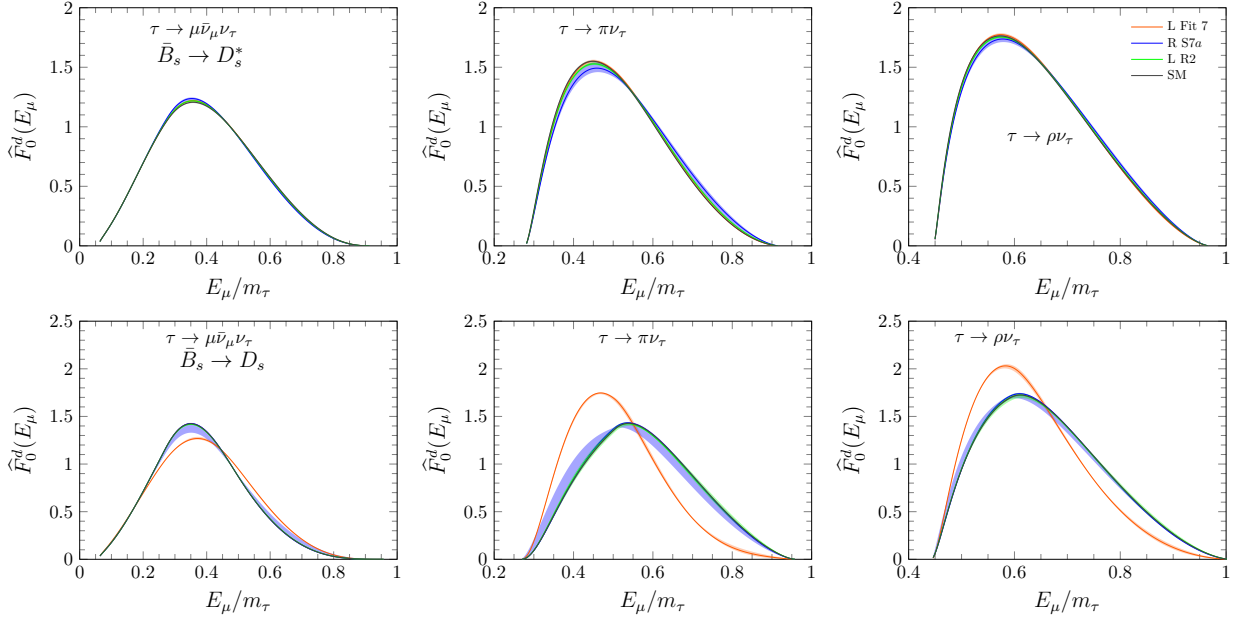


FIG. 11. \widehat{F}_0^d distribution (Eq. (37)) for the $\bar{B}_s \rightarrow D_s^{(*)} \tau^-(\pi^-\nu_\tau, \rho^-\nu_\tau, \mu^-\bar{\nu}_\mu\nu_\tau)\bar{\nu}_\tau$ sequential decays.

IV. SUMMARY

We have used the results of lattice evaluation of the SM form factors for the $\bar{B}_s \rightarrow D_s^{(*)}$ semileptonic decays in Refs. [31, 32] and their HQET expansions in Ref. [33] to obtain in addition the scalar, pseudoscalar and tensor form factors also needed for an analysis of NP effects on both semileptonic decays. We have compared results evaluated within the SM and three different NP extensions that have been previously used in the study of other CC $b \rightarrow c$ transitions. We find effects similar to those obtained for the SU(3)-analogue $\bar{B} \rightarrow D^{(*)}$ decays. We have evaluated the corresponding \mathcal{R}_{D_s} and $\mathcal{R}_{D_s^*}$ ratios which, as in the $\bar{B} \rightarrow D^{(*)}$ case, should be the easiest LFUV observable to measure. We have also analyzed the role that different tau asymmetries in the $\bar{B}_s \rightarrow D_s^{(*)} \tau^-\bar{\nu}_\tau$ decay could play, not only in establishing the existence of NP, but also in distinguishing between different NP

extensions of the SM. We have studied partially integrated angular and energy distributions of the charged particle produced in the subsequent $\tau^- \rightarrow \pi^- \nu_\tau$, $\rho^- \nu_\tau$, $e^- (\mu^-) \bar{\nu}_{e(\mu)} \nu_\tau$ decays. The latter differential decay widths have a better statistics than the asymmetries themselves and they could also help in establishing the presence of NP beyond the SM.

If NP is responsible for LFUV it should show up in $\bar{B}_s \rightarrow D_s^{(*)}$ semileptonic decays at the same level as for the $\bar{B} \rightarrow D^{(*)}$ ones. The analysis of this transition, as well of other CC $b \rightarrow c$ mediated decays, could then help in establishing or ruling out LFUV.

ACKNOWLEDGEMENTS

N.P. thanks Physics and Astronomy at the University of Southampton for hospitality during the making of this work and a Generalitat Valenciana grant CIBAFP/2021/32. This research has been supported by the Spanish Ministerio de Ciencia e Innovación (MICINN) and the European Regional Development Fund (ERDF) under contracts PID2020-112777GB-I00 and PID2019-105439GB-C22, the EU STRONG-2020 project under the program H2020-INFRAIA-2018-1, grant agreement no. 824093 and by Generalitat Valenciana under contract PROMETEO/2020/023.

Appendix A: Mean values and covariance matrices of the a_i^F coefficients in Eqs. (10)-(13).

As discussed in the main text, for our HQSS fit of the form factors we change the parametrizations in Refs. [31, 32] and adopt a new one to symmetrize the range of variation of the conformal variable z . Hence, we have expanded the SM form-factors as detailed in Eqs. (10) and (12). Statistical details of the new coefficients are collected here in Tables VI–XVII. Both sets of coefficients are related by linear transformations, making it straightforward to obtain new mean values and covariance matrices from the Gaussian means, errors and correlation matrices given in Refs. [31, 32] for the coefficients of the conformal expansions employed in those LQCD works. For each entry in the tables below, we provide three significant digits but neglect order 10^{-5} or smaller.

a_0^0	a_1^0	a_2^0	a_0^+	a_1^+
0.674 ± 0.009	-0.238 ± 0.218	-0.13 ± 1.61	0.764 ± 0.018	-3.04 ± 0.43
1.000	0.117	-0.074	0.567	-0.011
	1.000	-0.062	0.421	-0.030
		1.000	-0.145	0.229
			1.000	-0.726
				1.000

TABLE VI. Central values and errors (first row) of the $a_i^{0,+}$ coefficients of the new $f_{+,0}$ parametrization introduced in Eq. (12) and their corresponding correlation matrix. Note that a_2^+ is fixed through the condition $f_0(0) = f_+(0)$.

-
- [1] J. P. Lees *et al.* (BaBar), *Phys. Rev. Lett.* **109**, 101802 (2012), arXiv:1205.5442 [hep-ex].
 - [2] J. P. Lees *et al.* (BaBar), *Phys. Rev. D* **88**, 072012 (2013), arXiv:1303.0571 [hep-ex].
 - [3] M. Huschle *et al.* (Belle), *Phys. Rev. D* **92**, 072014 (2015), arXiv:1507.03233 [hep-ex].
 - [4] Y. Sato *et al.* (Belle), *Phys. Rev. D* **94**, 072007 (2016), arXiv:1607.07923 [hep-ex].

	A_0	A_1	A_2	V
a_0	0.0927 ± 0.0054	0.0549 ± 0.0025	0.0559 ± 0.0090	0.0946 ± 0.0101
a_1	-0.436 ± 0.128	-0.0118 ± 0.0572	-0.122 ± 0.211	-0.183 ± 0.271
a_2	-0.091 ± 0.966	-0.028 ± 0.769	-0.245 ± 0.787	0.00 ± 1.00
a_3	-0.020 ± 0.994	0.065 ± 0.986		0.000 ± 0.995

TABLE VII. Central values and errors of the a_i^F coefficients of the new parametrization (z^* -expansion) introduced in Eq. (10) for the A_0, A_1, A_2 and V form-factors. Note that $a_3^{A_2}$ is fixed by the condition in Eq. (5).

	$a_0^{A_0}$	$a_1^{A_0}$	$a_2^{A_0}$	$a_3^{A_0}$
$a_0^{A_0}$	1.000	0.234	0.0208	0.0003
$a_1^{A_0}$	0.234	1.000	0.250	0.0069
$a_2^{A_0}$	0.0208	0.250	1.000	0.0300
$a_3^{A_0}$	0.0003	0.0069	0.0300	1.000

TABLE VIII. Correlation matrix for the z^* -expansion coefficients of A_0 .

- [5] S. Hirose *et al.* (Belle), *Phys. Rev. Lett.* **118**, 211801 (2017), arXiv:1612.00529 [hep-ex].
- [6] G. Caria *et al.* (Belle), *Phys. Rev. Lett.* **124**, 161803 (2020), arXiv:1910.05864 [hep-ex].
- [7] R. Aaij *et al.* (LHCb), *Phys. Rev. Lett.* **115**, 111803 (2015), [Erratum: *Phys.Rev.Lett.* 115, 159901 (2015)], arXiv:1506.08614 [hep-ex].
- [8] R. Aaij *et al.* (LHCb), *Phys. Rev. Lett.* **120**, 171802 (2018), arXiv:1708.08856 [hep-ex].
- [9] R. Aaij *et al.* (LHCb), *Phys. Rev. D* **97**, 072013 (2018), arXiv:1711.02505 [hep-ex].
- [10] R. Aaij *et al.* (LHCb), arXiv:2302.02886 [hep-ex].
- [11] Y. S. Amhis *et al.* (HFLAV), *Eur. Phys. J. C* **81**, 226 (2021), arXiv:1909.12524 [hep-ex].
- [12] Resmi Puthumanaim (on behalf of the LHCb collaboration) CERN Seminar March 21, 2023.
- [13] R. Aaij *et al.* (LHCb), *Phys. Rev. Lett.* **120**, 121801 (2018), arXiv:1711.05623 [hep-ex].
- [14] A. Y. Anisimov, I. M. Narodetsky, C. Semay, and B. Silvestre-Brac, *Phys. Lett.* **B452**, 129 (1999), arXiv:hep-ph/9812514 [hep-ph].
- [15] M. A. Ivanov, J. G. Korner, and P. Santorelli, *Phys. Rev.* **D73**, 054024 (2006), arXiv:hep-ph/0602050 [hep-ph].
- [16] E. Hernández, J. Nieves, and J. Verde-Velasco, *Phys. Rev. D* **74**, 074008 (2006), arXiv:hep-ph/0607150.
- [17] T. Huang and F. Zuo, *Eur. Phys. J.* **C51**, 833 (2007), arXiv:hep-ph/0702147 [HEP-PH].
- [18] W. Wang, Y.-L. Shen, and C.-D. Lu, *Phys. Rev.* **D79**, 054012 (2009), arXiv:0811.3748 [hep-ph].
- [19] W.-F. Wang, Y.-Y. Fan, and Z.-J. Xiao, *Chin. Phys.* **C37**, 093102 (2013), arXiv:1212.5903 [hep-ph].
- [20] R. Watanabe, *Phys. Lett. B* **776**, 5 (2018), arXiv:1709.08644 [hep-ph].
- [21] A. Issadykov and M. A. Ivanov, *Phys. Lett.* **B783**, 178 (2018), arXiv:1804.00472 [hep-ph].
- [22] C.-T. Tran, M. A. Ivanov, J. G. Körner, and P. Santorelli, *Phys. Rev.* **D97**, 054014 (2018), arXiv:1801.06927 [hep-ph].
- [23] X.-Q. Hu, S.-P. Jin, and Z.-J. Xiao, *Chin. Phys.* **C44**, 023104 (2020), arXiv:1904.07530 [hep-ph].
- [24] D. Leljak, B. Melic, and M. Patra, *JHEP* **05**, 094 (2019), arXiv:1901.08368 [hep-ph].
- [25] K. Azizi, Y. Sarac, and H. Sundu, *Phys. Rev.* **D99**, 113004 (2019), arXiv:1904.08267 [hep-ph].
- [26] W. Wang and R. Zhu, *Int. J. Mod. Phys. A* **34**, 1950195 (2019), arXiv:1808.10830 [hep-ph].
- [27] R. Aaij *et al.* (LHCb), (2022), arXiv:2201.03497 [hep-ex].
- [28] W. Detmold, C. Lehner, and S. Meinel, *Phys. Rev.* **D92**, 034503 (2015), arXiv:1503.01421 [hep-lat].
- [29] Marco Pappagallo (LHCb deputy physics coordinator) private communication.
- [30] Y. S. Amhis *et al.* (HFLAV), *Phys. Rev. D* **107**, 052008 (2023), arXiv:2206.07501 [hep-ex].
- [31] E. McLean, C. T. H. Davies, J. Koponen, and A. T. Lytle, *Phys. Rev. D* **101**, 074513 (2020), arXiv:1906.00701 [hep-lat].

	$a_0^{A_0}$	$a_1^{A_0}$	$a_2^{A_0}$	$a_3^{A_0}$
$a_0^{A_1}$	0.253	-0.0029	0.0209	0.0032
$a_1^{A_1}$	-0.0337	-0.128	0.0744	0.0089
$a_2^{A_1}$	-0.0228	-0.192	0.0534	0.0259
$a_3^{A_1}$	-0.0035	-0.0201	-0.0054	0.0057

TABLE IX. Correlation matrix for the z^* -expansion coefficients of A_0 and A_1 .

	$a_0^{A_0}$	$a_1^{A_0}$	$a_2^{A_0}$	$a_3^{A_0}$
$a_0^{A_2}$	-0.471	-0.253	0.0163	0.0028
$a_1^{A_2}$	-0.0267	-0.532	-0.215	0.0032
$a_2^{A_2}$	0.0231	0.182	-0.0183	-0.0342

TABLE X. Correlation matrix for the z^* -expansion coefficients of A_0 and A_2 .

- [32] J. Harrison and C. T. H. Davies (HPQCD), *Phys. Rev. D* **105**, 094506 (2022), arXiv:2105.11433 [hep-lat].
- [33] F. U. Bernlochner, Z. Ligeti, M. Papucci, and D. J. Robinson, *Phys. Rev.* **D95**, 115008 (2017), [erratum: *Phys. Rev.*D97,no.5,059902(2018)], arXiv:1703.05330 [hep-ph].
- [34] M. E. Luke, *Phys. Lett. B* **252**, 447 (1990).
- [35] C. Murgui, A. Penñelas, M. Jung, and A. Pich, *JHEP* **09**, 103 (2019), arXiv:1904.09311 [hep-ph].
- [36] M. Jung and D. M. Straub, *JHEP* **01**, 009 (2019), arXiv:1801.01112 [hep-ph].
- [37] N. Penalva, E. Hernández, and J. Nieves, *JHEP* **06**, 118 (2021), arXiv:2103.01857 [hep-ph].
- [38] N. Penalva, E. Hernández, and J. Nieves, *JHEP* **10**, 122 (2021), arXiv:2107.13406 [hep-ph].
- [39] R. Alonso, A. Kobach, and J. Martin Camalich, *Phys. Rev. D* **94**, 094021 (2016), arXiv:1602.07671 [hep-ph].
- [40] R. Alonso, J. Martin Camalich, and S. Westhoff, *Phys. Rev. D* **95**, 093006 (2017), arXiv:1702.02773 [hep-ph].
- [41] P. Asadi, A. Hallin, J. Martin Camalich, D. Shih, and S. Westhoff, *Phys. Rev. D* **102**, 095028 (2020), arXiv:2006.16416 [hep-ph].
- [42] N. Penalva, E. Hernández, and J. Nieves, *JHEP* **04**, 026 (2022), arXiv:2201.05537 [hep-ph].
- [43] N. Penalva, E. Hernández, and J. Nieves, *Phys. Rev. D* **101**, 113004 (2020), arXiv:2004.08253 [hep-ph].
- [44] N. Penalva, E. Hernández, and J. Nieves, *Phys. Rev. D* **102**, 096016 (2020), arXiv:2007.12590 [hep-ph].
- [45] S. Fajfer, J. F. Kamenik, and I. Nisandzic, *Phys. Rev.* **D85**, 094025 (2012), arXiv:1203.2654 [hep-ph].
- [46] A. Abdesselam *et al.* (Belle), in *10th International Workshop on the CKM Unitarity Triangle* (2019) arXiv:1903.03102 [hep-ex].
- [47] R. Alonso, B. Grinstein, and J. Martin Camalich, *Phys. Rev. Lett.* **118**, 081802 (2017), arXiv:1611.06676 [hep-ph].
- [48] U. Nierste, S. Trine, and S. Westhoff, *Phys. Rev. D* **78**, 015006 (2008), arXiv:0801.4938 [hep-ph].
- [49] M. Tanaka and R. Watanabe, *Phys. Rev. D* **87**, 034028 (2013), arXiv:1212.1878 [hep-ph].
- [50] M. Duraisamy and A. Datta, *JHEP* **09**, 059 (2013), arXiv:1302.7031 [hep-ph].
- [51] M. Duraisamy, P. Sharma, and A. Datta, *Phys. Rev. D* **90**, 074013 (2014), arXiv:1405.3719 [hep-ph].
- [52] D. Becirevic, S. Fajfer, I. Nisandzic, and A. Tayduganov, *Nucl. Phys. B* **946**, 114707 (2019), arXiv:1602.03030 [hep-ph].
- [53] Z. Ligeti, M. Papucci, and D. J. Robinson, *JHEP* **01**, 083 (2017), arXiv:1610.02045 [hep-ph].
- [54] M. A. Ivanov, J. G. Körner, and C.-T. Tran, *Phys. Rev. D* **95**, 036021 (2017), arXiv:1701.02937 [hep-ph].
- [55] M. Blanke, A. Crivellin, S. de Boer, T. Kitahara, M. Moscati, U. Nierste, and I. Nišandžić, *Phys. Rev.* **D99**, 075006 (2019), arXiv:1811.09603 [hep-ph].

	$a_0^{A_0}$	$a_1^{A_0}$	$a_2^{A_0}$	$a_3^{A_0}$
a_0^V	-0.0041	0.0131	0.0005	0.0002
a_1^V	-0.0046	0.0140	0.0034	0
a_2^V	0	0.0005	0.0003	0
a_3^V	0	0	0	0

TABLE XI. Correlation matrix for the z^* -expansion coefficients of A_0 and V .

	$a_0^{A_1}$	$a_1^{A_1}$	$a_2^{A_1}$	$a_3^{A_1}$
$a_0^{A_1}$	1.	0.502	0.0368	-0.0107
$a_1^{A_1}$	0.502	1.	0.454	-0.0211
$a_2^{A_1}$	0.0368	0.454	1.	-0.0288
$a_3^{A_1}$	-0.0107	-0.0211	-0.0288	1.

TABLE XII. Correlation matrix for the z^* -expansion coefficients of A_1 .

- [56] S. Bhattacharya, S. Nandi, and S. Kumar Patra, *Eur. Phys. J. C* **79**, 268 (2019), arXiv:1805.08222 [hep-ph].
- [57] P. Colangelo and F. De Fazio, *JHEP* **06**, 082 (2018), arXiv:1801.10468 [hep-ph].
- [58] R.-X. Shi, L.-S. Geng, B. Grinstein, S. Jäger, and J. Martin Camalich, *JHEP* **12**, 065 (2019), arXiv:1905.08498 [hep-ph].
- [59] A. K. Alok, D. Kumar, S. Kumbhakar, and S. Uma Sankar, *Nucl. Phys. B* **953**, 114957 (2020), arXiv:1903.10486 [hep-ph].
- [60] R. Mandal, C. Murgui, A. Peñuelas, and A. Pich, *JHEP* **08**, 022 (2020), arXiv:2004.06726 [hep-ph].
- [61] S. Kumbhakar, *Nucl. Phys. B* **963**, 115297 (2021), arXiv:2007.08132 [hep-ph].
- [62] S. Iguro and R. Watanabe, *JHEP* **08**, 006 (2020), arXiv:2004.10208 [hep-ph].
- [63] B. Bhattacharya, A. Datta, S. Kamali, and D. London, *JHEP* **07**, 194 (2020), arXiv:2005.03032 [hep-ph].
- [64] R. Dutta and A. Bhol, *Phys. Rev. D* **96**, 076001 (2017), arXiv:1701.08598 [hep-ph].
- [65] J. Harrison, C. T. Davies, and A. Lytle (LATTICE-HPQCD), *Phys. Rev. Lett.* **125**, 222003 (2020), arXiv:2007.06956 [hep-lat].
- [66] R. Dutta, *Phys. Rev. D* **93**, 054003 (2016), arXiv:1512.04034 [hep-ph].
- [67] S. Shivashankara, W. Wu, and A. Datta, *Phys. Rev. D* **91**, 115003 (2015), arXiv:1502.07230 [hep-ph].
- [68] X.-Q. Li, Y.-D. Yang, and X. Zhang, *JHEP* **02**, 068 (2017), arXiv:1611.01635 [hep-ph].
- [69] A. Datta, S. Kamali, S. Meinel, and A. Rashed, *JHEP* **08**, 131 (2017), arXiv:1702.02243 [hep-ph].
- [70] A. Ray, S. Sahoo, and R. Mohanta, *Phys. Rev. D* **99**, 015015 (2019), arXiv:1812.08314 [hep-ph].
- [71] T. Gutsche, M. A. Ivanov, J. G. Körner, V. E. Lyubovitskij, P. Santorelli, and C.-T. Tran, *Phys. Rev. D* **98**, 053003 (2018), arXiv:1807.11300 [hep-ph].
- [72] F. U. Bernlochner, Z. Ligeti, D. J. Robinson, and W. L. Sutcliffe, *Phys. Rev. D* **99**, 055008 (2019), arXiv:1812.07593 [hep-ph].
- [73] E. Di Salvo, F. Fontanelli, and Z. J. Ajaltouni, *Int. J. Mod. Phys. A* **33**, 1850169 (2018), arXiv:1804.05592 [hep-ph].
- [74] M. Blanke, A. Crivellin, T. Kitahara, M. Moscati, U. Nierste, and I. Nišandžić, *Phys. Rev. D* **100**, 035035 (2019), arXiv:1905.08253 [hep-ph].
- [75] P. Böer, A. Kokulu, J.-N. Toelstede, and D. van Dyk, (2019), arXiv:1907.12554 [hep-ph].
- [76] X.-L. Mu, Y. Li, Z.-T. Zou, and B. Zhu, *Phys. Rev. D* **100**, 113004 (2019), arXiv:1909.10769 [hep-ph].
- [77] Q.-Y. Hu, X.-Q. Li, Y.-D. Yang, and D.-H. Zheng, *JHEP* **02**, 183 (2021), arXiv:2011.05912 [hep-ph].
- [78] N. Penalva, E. Hernández, and J. Nieves, *Phys. Rev. D* **100**, 113007 (2019), arXiv:1908.02328 [hep-ph].
- [79] F. U. Bernlochner, Z. Ligeti, M. Papucci, and D. J. Robinson, (2022), arXiv:2206.11282 [hep-ph].
- [80] A. K. Leibovich and I. W. Stewart, *Phys. Rev. D* **57**, 5620 (1998), arXiv:hep-ph/9711257.

	$a_0^{A_1}$	$a_1^{A_1}$	$a_2^{A_1}$	$a_3^{A_1}$
$a_0^{A_2}$	0.634	0.519	-0.0055	-0.0040
$a_1^{A_2}$	0.0874	0.479	0.625	-0.0109
$a_2^{A_2}$	0.0812	0.223	0.501	0.0948

TABLE XIII. Correlation matrix for the z^* -expansion coefficients of A_1 and A_2 .

	$a_0^{A_1}$	$a_1^{A_1}$	$a_2^{A_1}$	$a_3^{A_1}$
a_0^V	0.0329	0.0342	0.0115	-0.0013
a_1^V	0.0248	0.0320	0.0168	-0.0002
a_2^V	0.0012	0.0012	0.0007	0
a_3^V	0	0	0	0

TABLE XIV. Correlation matrix for the z^* -expansion coefficients of A_1 and V .

- [81] M. Papucci and D. J. Robinson, *Phys. Rev. D* **105**, 016027 (2022), arXiv:2105.09330 [hep-ph].
- [82] M.-L. Du, E. Hernández, and J. Nieves, *Phys. Rev. D* **106**, 114020 (2022), arXiv:2207.02109 [hep-ph].
- [83] J. Nieves and R. Pavao, *Phys. Rev. D* **101**, 014018 (2020), arXiv:1907.05747 [hep-ph].
- [84] P. Böer, M. Bordone, E. Graverini, P. Owen, M. Rotondo, and D. Van Dyk, *JHEP* **06**, 155 (2018), arXiv:1801.08367 [hep-ph].
- [85] J. Nieves, R. Pavao, and S. Sakai, *Eur. Phys. J. C* **79**, 417 (2019), arXiv:1903.11911 [hep-ph].
- [86] S. Meinel and G. Rendon, *Phys. Rev. D* **103**, 094516 (2021), arXiv:2103.08775 [hep-lat].
- [87] M.-L. Du, N. Penalva, E. Hernández, and J. Nieves, *Phys. Rev. D* **106**, 055039 (2022), arXiv:2207.10529 [hep-ph].

	$a_0^{A_2}$	$a_1^{A_2}$	$a_2^{A_2}$
$a_0^{A_2}$	1.	-0.0849	0.0829
$a_1^{A_2}$	-0.0849	1.	-0.0141
$a_2^{A_2}$	0.0829	-0.0141	1.

TABLE XV. Correlation matrix for the z^* -expansion coefficients of A_2 . We use Eq. (5) to fix the $a_3^{A_2}$ coefficient for $\bar{B}_s \rightarrow D_s^*$ decay.

	$a_0^{A_2}$	$a_1^{A_2}$	$a_2^{A_2}$
a_0^V	0.0128	0.0317	0.0020
a_1^V	-0.0014	0.0457	-0.0031
a_2^V	0.0002	0.0014	0.0001
a_3^V	0	0	0

TABLE XVI. Correlation matrix for the z^* -expansion coefficients of A_2 and V .

	a_0^V	a_1^V	a_2^V	a_3^V
a_0^V	1.	0.252	0.0133	-0.0003
a_1^V	0.252	1.	0.0927	-0.0001
a_2^V	0.0133	0.0927	1.	0.0275
a_3^V	-0.0003	-0.0001	0.0275	1.

TABLE XVII. Correlation matrix for the z^* -expansion coefficients of V .